Alpha heating, isotopic mass, and fast ion effects in deuterium-tritium experiments

R.V. Budny[1,a,*] and JET contributors[a]
EUROfusion Consortium, JET, Culham Science Centre, Abingdon, OX14 3DB, UK
[1] *Princeton University, (retired), Princeton, NJ 08540, USA*
(Dated: July 25, 2018)

Alpha heating experiments in the Tokamak Fusion Test Reactor (TFTR) and in the Joint European Torus (JET) 1997 DTE1 campaign are reexamined. In TFTR supershots central electron heating of both deuterium only and deuterium - tritium supershots was dominated by thermal ion-electron heat transfer rate $p_{\rm ie}$ The higher T_e in deuterium-tritium supershots was mainly due to higher T_i largely caused by isotopic mass effects of neutral beam - thermal ion heating. The thermal ion - electron heating dominated the electron heating in the center. The ratio of the predicted alpha to total electron heating rates $f_{\rm alp}$ is less than 0.30. Thus alpha heating (and possible favorable isotopic mass scaling of the thermal plasma) were too small to be measured reliably.

The JET alpha heating Hot-Ion H-mode discharges had lower T_i/T_e, and thus had lower $p_{\rm ie}$ and the deuterium - tritium DT discharges had higher $f_{\rm alp}$ than in TFTR. There weren't enough comparable discharges to verify alpha heating. The high performance phases consisted of rampup to brief flattop durations. At equal times during the rampup phase central T_e and T_i were linearly correlated with the thermal hydrogenic isotopic mass $< A >_{\rm hyd}$ which co-varied with beam ion pressure, the tritium fraction of neutral beam power, and the time delay to the first significant sawteeth which interrupted the T_e increases.

For both devices the expected alpha heating rate and the null hypothesis of no alpha heating are consistent with the measurements within the measurement and modeling uncertainties.

Keywords: tokamak experiments, TFTR, JET, deuterium and tritium, alpha heating, isotopic mass effects, fast ion effects

(Some figures may appear in colour only in the online journal)

1. Introduction

Alpha heating is essential for practical energy production from DT fusion reactions. Experiments to detect alpha heating were performed in TFTR (1994) [1, 2] and in the JET DTE1 campaign (1997) [3, 4]. In these discharges the tritium content was varied by varying the T fraction in the neutral beam NB injection and in the gas puffing, and wall conditioning.

The TFTR DT experiments led to the conclusions that alpha particle heating of electrons was consistent with measurements, and that ion temperature T_i and confinement in the center strongly correlated with the thermal hydrogenic isotopic mass, $< A >_{\rm hyd} \equiv (n_{\rm H} + 2n_{\rm D} + 3n_{\rm T})/(n_{\rm H} + n_{\rm D} + n_{\rm T})$ where n_j are the densities of the thermal H (trace), D, and T. The JET experiments led to the conclusion that alpha heating had been unambiguously observed.

This paper argues that the null hypothesis of no alpha heating is also consistent with the measurements. We identify the main cause of high central T_e in TFTR supershots as the high thermal ion - electron energy exchange rate $p_{\rm ie}$ resulting from high T_i/T_e. The higher T_i and thus higher T_e in deuterium - tritium DT supershots is due to effects stemming from the isotopic mass of the NB heating. This mass is quantified by the ratio $f_{\rm NBT}$ of the NB power injected as tritium $P_{\rm NBT}$ to the total power $P_{\rm NB}$. Analysis of both the TFTR and JET plasmas show that the values near the magnatic axis of $< A >_{\rm hyd}$ are related to $f_{\rm NBT}$ by [5]

$$< A >_{\rm hyd} \lesssim f_{\rm NBT} + 2 \tag{1}$$

which is plausible since beam fueling is the dominant hydrogenic species source in the center. This connection

complicates experimental separation of possible isotopic effects on T_e and T_i from the thermal plasma or the beam injection.

Early analysis of the JET results led to the conclusions that isotopic scaling of core parameters was not observed. The central T_e and T_i did not increase as consistently with either the calculated central alpha particle or alpha heating rate densities. This conclusion of no isotopic effects required additional explanations of the observed larger core T_i in DT compared with DD plasmas (D NBI into D thermal plasmas). Possible mechanisms proposed [4, 6] included fast ion stabilization of turbulence and changes in confinement induced by the presence of alpha particles.

This paper also extends the reanalysis of the JET alpha heating experiment in [5] to consider effects of the beam isotopic mass and additional variables. The central beam ion heating rates did scale with the beam isotopic mass, but since T_i/T_e was less than in TFTR, $p_{\rm ie}$ was less dominant. The increase of the delay to significant sawteeth with increasing isotopic mass had a significant effect on T_e which complicated the analysis. It remains ambiguous whether the isotopic mass of the thermal plasma $< A >_{\rm hyd}$ or of the NB injection $f_{\rm NBT}$ is the main cause of higher T_e in DT. Due to the scarcity of comparable discharges, poorly-matched DD and DT discharges were sometimes compared.

Early analysis of the alpha heating experiments [1–4, 6] focused on comparisons of T_e in the core of DT and DD discharges. This focus is misleading since there is no guarantee that the additional alpha heating won't degrade electron energy confinement instead of increasing T_e. This would be unfortunate for controlled fusion energy. Quantifying alpha heating requires study of energy balance of the electron stored energy $w_{\rm e}$. The alpha-electron heating rate $p_{\alpha e}$ should be compared with other, potentially larger rates.

One of the goals of this paper is to show why alpha heating was difficult to quantify experimentally in order to help future attempts. Alpha heating experiments are planned for JET in 2019-2020 and in ITER starting after 2035. It is instructive to reconsider the TFTR along with the JET alpha heating experiments since the plasma regimes and difficulties contrast each other. Understanding both helps generalize to upcoming experiments. For instance the synergistic coupling of ion and electron energy described in Section 2.4 occurs in both Tokamaks but is clearer in the TFTR data.

2. TFTR

2.1 Description of discharges

We focus on a well-matched triplet consisting of a DD and two DT supershots. The analysis and results generalize to other DT supershots. One of the DT supershots in the triplet had the highest known ratio of the predicted alpha to total electron heating rate $p_{\rm e}$: $p_{\alpha e}/p_{\rm e} \equiv f_{\rm alp}$. These had well-conditioned first walls resulting from Li pellets injected before the neutral beam NB phase. The wall conditioning resulted in low $n_{\rm e}$ carbon-rich plasmas at the start of NB. The line-averaged electron density $\overline{n}_{\rm e}$ increased during the NB phase starting at 14% of the Greenwald empirical limit $\overline{n}_{\rm Gw} = I_p/(\pi a^2)\ MA/m^2$ [7, 8] to a peak of 27%. It is not clear if this empirical density limit is relevant for the highly peaked profiles of supershots. The Li wall conditioning decreased $\overline{n}_{\rm e}$ at the start of NB.

The lower edge density caused deeper NB penetration and higher energy confinement [9]. Trace amounts of Li from the pellet fragments appear to have been in the core at least at the start of NB. Large rates of line emission at 119 $\mathring{A}$ were seen in similar supershots suggesting the presence of Li^+ with temperatures in the range of a few to tens of eV [10].

The triplet had moderate NB power $P_{\rm nb} = 13.8$ MW. The flattop plasma current was 2.3 MA and the toroidal field = 5.5 Tesla. The DT discharges had global and local (near the magnetic axis) fusion energy gains defined as the ratios of the total and central fusion power $P_{\rm DT}$ divided by the auxiliary heating power using their global or central values respectively [11], $Q_{\rm DT}$ = 0.17-0.18 and $q_{\rm DT} = 0.4$ during the NB phase. Some supershots achieved higher $Q_{\rm DT}$, $q_{\rm DT}$, and $p_{\alpha e}$ but did not have matching DD discharges. An example is the supershot with record $Q_{\rm DT}$ (= 0.28) which had central $q_{\rm DT} \simeq 0.8$ with alpha-electron heating rate $p_{\alpha e} = 0.23$ MW/m^3 [11] . A summary of various parameters for noteworthy discharges is given in table 1.

Waveforms for the triplet are shown in figure 1. The beam powers in figure 1-a) show a transient occurring early in the DD discharge. In the experiments in TFTR and JET during the days with T NB injection generally all the

NB beamlines were tuned for T at the expense of optimal D NB. This caused the D power waveforms to be choppy compared with those with T NB. Thus pairs of DD and DT discharges with well matched total beam powers could rarely be found during the same run days. Transient drops in the beam power caused the core T_e to drop for durations longer than the dropout durations. Thus the best matched pairs vis-a-vis $P_{\rm nb}$ came from different days when tokamak wall conditions typically had varied. The DT supershots considered here occurred the day after the DD supershot. The transient in the DD $P_{\rm nb}$ waveform in this case was sufficiently early to not severely compromise comparisons.

The fraction of $P_{\rm nb}$ with tritium $f_{\rm NBT}$ was 0.66 for both DT supershots in the triplet. Experiments showed that fractions around this value maximized the neutron emission rates. Several supershots were created having small levels of $P_{\rm nb}$ for CX measurements after the main heating phase. The DD and one of the DT discharges had two brief 'beam blips' of $P_{\rm NB}$ after the main phase. The other DT had reduced $P_{\rm NB}$ after the main phase. The rational for these was to extend the window of charge-exchange spectroscopy (CX) data for better analysis in the late phase when alpha heating was expected to be relatively large.

The central electron density should be well matched for good comparisons. The central $n_{\rm e}$ evolution is shown in figure 1-b). The central beam electron fueling rate $s_{\rm be}$ was 5-10% higher for the DT supershots due to deeper T beam penetration. The beam-fueling rates for both the DD and DT supershots decreased rapidly after NB termination, as typically seen in TFTR.

High central $n_{\rm e}$ caused high central $n_{\rm D}$ and/or $n_{\rm T}$ permitting high $p_{\alpha e}$. In supershots high central $n_{\rm e}$ resulted from high $P_{\rm nb}$ and high central pressure, with disruption-caused limits. In JET Hot-ion H-mode discharges the central $n_{\rm e}$ tended to continue increasing after NB termination.

2.2 T_e Afterglow

The highest T_e measured in TFTR (from electron-cyclotron emission) were $\simeq$14 keV. The X-mode second harmonic optical depth was much higher even in the afterglow so higher harmonic pollution was not an issue [12]. These highest values occurred in discharges with much higher T_i ($\simeq$45 keV). The central T_e evoluions for the triplet shown in figure 1-c) are significantly higher for the DT discharges. The highest T_e were transient increases in the core region following termination or reduction of NB in supershots with high T_e during the NB phase. These were dubbed "afterglows', and were typically seen unless a major disruption forced rapid termination of the plasma.

There has been speculation that alpha heating had a significant role in energy balance during afterglows. One reason this hasn't been studied previously is that CX data needed for T_i and rotation profiles exists only when the beamlines used for the diagnostic were injecting power. These measurements are needed for credible modeling. The triplet discharges did have late CX data which are used here.

The calculated alpha heating usually increased with time during the discharges. The steady state phases did not last much longer than the alpha slowing down time (around 0.5-1.0s in TFTR and 1-1.5s in the JET alpha heating discharges). For this reason, and since the other electron heating decreased after NB termination, the ratio of alpha heating $f_{\rm alp}$ to total electron heating was maximum at late times. Here we study energy balance in the core during both the main heating phase and the lower power phases when CX data was available.

Afterglows were also seen in DD supershots as shown in the figure figure 1-c) with ΔT_e smaller than in DT. Afterglows occurred when T_e and T_i were high, and when and only when the very peaked (ubiquitous in supershots) central electron density $n_{\rm e}$ decreased, with a dependence of $\Delta T_e \propto -\frac{d}{dt}(n_{\rm e})$. Core $n_{\rm e}$ were strongly and linearly correlated with $P_{\rm NB}$ since beam fueling of electrons was by far the largest electron source in the core.

Afterglows were not seen in the JET alpha heating discharges, most of which had increasing $n_{\rm e}$, as discussed in the next Section. The occurrence of two afterglows seen in the TFTR 89402 supershot from the triplet (figure 1-c) were unusual, resulting from the two decreases in $P_{\rm NB}$ and thus core $n_{\rm e}$. A DD supershot (89387) similar to 89402 but with 12% lower $P_{\rm NB}$ and 19% lower $n_{\rm e}$ had two weaker afterglows at the smaller decreases in $n_{\rm e}$. Three afterglows were seen in a supershot (DT 83545), two caused by MHD events which lowered $n_{\rm e}$ and one by NB termination.

The central electron energy density $w_{\rm e}$ (pressure) are shown in figure 1-d). Afterglow-like bumps were not seen in the core $w_{\rm e}$. The central electron heating rate decreased for the afterglows, as is shown below, so TRANSP analysis shows a moderate decrease of the electron conductivity $\chi_{\rm e}$ (computed from the ratio of the energy fluxes and the

temperature gradient) in the afterglow region.

Sawteeth were suppressed during the main heating phase, but reappear later. Figure 1-c) shows the typical reappearance seen in TFTR and JET, with a time delay being longer in DT than in DD. In JET sawtooth crashes during the main heating phase had significant consequences complicating measurement of alpha heating, as discussed below.

2.3 High T_i

Supershots had especially high temperatures T_c measured by CX for the carbon impurity. Peak central values were often in the 40 - 50 keV range. The central T_c of the triplet, shown in figure 1-e), were lower due to the modest NB powers used. The peak T_c were 40% higher with DT. Typically the peak T_c values occurred within 0.5 s of the start of the NBI, whereas T_e peaked later. The T_c profiles at the first CX data time 4.025s (25 msec after the start of NB) are 18% higher in the DT supershots, indicating an isotopic mass effect.

The temperature of the bulk hydrogenic ions is calculated from T_c in TRANSP [13]. Its values are typically smaller than T_c at the highest values by $\simeq$ 5-10%. The CX data for the two triplet discharges with brief beam blips do not exist between the termination of the main NB phase and the blips.

Supershots had high toroidal rotation angular velocities Ω_{tor} measured for the carbon impurity. The DT discharges in the triplet were 40% higher than the DD, shown in figure 1-f). The highest carbon Mach numbers in the center were around unity. The Mach number for the hydrogenic ions computed by TRANSP from the carbon Ω_{tor} using NCLASS is around 0.5. Larger flow shearing rates in the DT plasmas caused by higher rotation rates might have caused greater turbulence suppression. Non-linear gyrokinetic simulations of the energy flows have been attempted, but haven't succeeded in predicting the measured energy transport in supershots.

The TRANSP inputs, modeling, and validity for TFTR are discussed in Appendix A. Excellent agreement is achieved simulating the measured neutron emission rates. This gives confidence in the predictions of the classical alpha heating and transport rates. Some of the supershot profiles were very peaked in the center. This had the benefit of creating very peaked alpha parameter profiles such as the alpha-electron heating rate $p_{\alpha e}$ with high central values. Unfortunately this peaking also caused uncertainties in the modeling due to systematic errors locating the plasma center in different diagnostics and modeling.

The thermal-ion electron heating rate $p_{\rm ie}$ is computed in TRANSP as proportional to the ratio of T_i-T_e to the thermal-ion electron energy exchange rate, $\propto T_e^{1.5}/n_{\rm e}$. This is the largest electron heating rate in the center of supershots and is typically at least three to four times the peak $p_{\alpha e}$ with DT. Dominant electron heating rates in the DT supershots in the triplet are compared in figure 2. The evolution of the dominant central values for 89402 are shown in figure 2-a). The ratio $f_{\rm alp}$ of $p_{\alpha e}$ to the total electron heating rate $p_{\rm e}$ is shown in figure 2-b). The highest values of $f_{\rm alp} \simeq 0.3$ are from the beam blips supershot in which systematic errors might be unusually large, as indicated in Appendix A. This is the largest $f_{\rm alp}$ computed for TFTR. Values for various discharges are shown in table 1.

Profiles of the dominant electron heating rates in 89402 are shown in figure 2-c, -d). The radial grid x consists of equally spaced square-root of the normalized toroidal flux, which is approximately the normalized minor radius. The times shown are the last CX data time in the main NB phase and the last (in the postlude phase). Subtle differences between the global and core $Z_{\rm eff}$ assumptions are discussed in Appendix A.

Profiles of the dominant electron heating rates in 89405 with beam blips are shown in figure 2-e, -f). The central T_i was considerably lower at that time, compared with 89402, and approximately equal to T_e, so $p_{\rm ie}$ was low. The central Ohmic heating rate dominated, however there are considerable uncertainties in this calculated rate. The results shown were calculated assuming NCLASS resitivity.

2.4 High T_i caused high T_e

Since $p_{\rm ie}$ generally dominated the electron heating in the center the important question is why is $T_i - T_e$ or alternatively the ratio T_i/T_e so large. This ratio is around 4 in supershots and 1.5 in the JET alpha heating discharges. In JET ELMy H-mode plasmas (with Edge localized modes) the ratio is ≈1.0. In JET H-modes the energy transport is stiff meaning that the temperature gradients are limited so high central temperatures require high pedestal temperatures. This is not true for T_i in TFTR supershots which have no pedestals. The lower the edge density the higher the central T_i due to improved penetration to the core in TFTR. The edge T_i in TFTR was rather consistently low ($\simeq$ a few hundred eV), and $T_i \simeq T_e$ into the half radius. Within the half radius T_i became very steep. Profiles are shown in Appendix A.

A hypothesis proposed during the TFTR experiments was that T_i/T_e is large due to a vary favorable intrinsic isotopic scaling of confinement in the thermal plasma seen clearly in T_i [1, 14–16]. The range of $< A >_{\rm hyd}$ accessed in TFTR was limited due to significant wall fueling of latent D emitted by the walls. Even though experiments with TT supershots were performed, the largest values for $< A >_{\rm hyd}$ were $\simeq$2.7. Typical DT and TT supershots had $< A >_{\rm hyd}$ below $\simeq$2.5. JET achieved values near 3.0. The early analysis [3] of the JET alpha heating set excluded the hypothesis of an isotopic mass effect partly based on the tritium beam injection into the tritium plasma TT outlier discharge 43011 [5].

Trajectories of central T_e vs T_i are shown in figure 3. Their values increase linearly with the same slope during the rampup to maximum T_i, then T_i saturated and T_e continued to increase. Later, their trajectories have a counter-clockwise rotation since the maximum T_e occurs after the time of maximum T_i. This would be expected from extra electron heating such as $p_{\alpha e}$ which should increase with time, but this upturn and rotation are also seen in the DD supershot 89364. If instead of rotating counter-clockwise after the peak T_i the trajectories flattened this would indicate that T_e had saturated reaching an upper bound. The trajectory for the record $Q_{\rm DT}$ supershot is also shown in figure 3-a).

High T_i and similar trajectories were also seen in the DD supershot conditioning scan discussed in [9]. Trajectories of central T_e vs T_i are shown in figure 3-b). These DD supershots had trace amounts of tritium but had negligible calculated $p_{\alpha e}$ and $< A >_{\rm hyd} \simeq 2$.

The beam ion heating rate of thermal ions $p_{\rm bi}$ is calculated in TRANSP as the sum of the heating of the thermal ions by beam ions as they slow down and by the energy they add to the thermal ion population after they thermalized. The cutoff energy is taken to be 1.5 times the local T_i. Evolution of the central $p_{\rm bi}$ are shown in figure 4-a), -b). The rate tended to increase slightly with $< A >_{\rm hyd}$ and $f_{\rm NBT}$ in the triplet and to increase dramatically with wall conditioning.

The time variations and isotopic mass variations of the central $p_{\rm bi}$ shown in figure 4-a) resemble the T_i variations shown in figure 1-e). Generally in supershots $p_{\rm bi}$ decreased in time after peaking early during NBI, even with constant $P_{\rm nb}$. Typically central $p_{\rm bi}$ and T_i both peaked within 350 ms after the start of NBI. Thus the large T_e and T_i in DT might be due simply to effects of the isotopic mass of the NB heating. A subtlety is that the core values of these isotopic masses are related to the NB species fueling by Eq. (1) since beam fueling is the dominate hydrogenic species source in the center. Thus experimentally distinguishing $< A >_{\rm hyd}$ and $f_{\rm NBT}$ is challenging. Analogous plots for the conditioning series are in figure 4-b).

The $p_{\rm ie}$ is a significant contributor to the net central thermal ion heating rate when $T_i \gg T_e$ as in the discharges studied. The thermal ion energy balance can be approximated by

$$p_{\rm i} \equiv p_{\rm bi} - p_{\rm ie} \simeq \frac{\partial w_{\rm i}}{\partial t} + p_{\rm cx} + p_{\rm i-conv} + p_{\rm i-cond} \qquad (2)$$

with $p_{\rm i}$ the effective thermal ion heating rate, $w_{\rm i}$ the thermal ion energy, $p_{\rm cx}$ the charge exchange net loss rate, and $p_{\rm i-conv} + p_{\rm i-cond}$ the convected and conducted thermal ion energy outflows. TRANSP computes additional terms which have relatively small values for the discharges without Ion Cyclotron IC heating. Thus, this is accurate for the discharges without IC heating studied here. Equation (2) is accurate over the whole TRANSP radial domain from the plasma center to the last-closed-flux surface. The radial profiles of $p_{\rm i}$ are very centrally peaked, as are the profiles of $w_{\rm i}$ and T_i discussed in Appendix A. The evolutions of the central values of $p_{\rm i}$ are shown in figure 4-c),-d).

Trajectories of the thermal ion energy density $w_{\rm i}$ versus the time-integral of $p_{\rm i}$ at the center are shown in figure 4-e),-f). The trajectory of the supershot with record $Q_{\rm DT}$ and $P_{\rm NB}$=40 MW is also shown. During the rampup to peak $p_{\rm i}$ the time integral of $p_{\rm i}$ tracks approximately the increase of $w_{\rm i}$. This indicates that the central thermal ion stored energy $w_{\rm i}$ was accumulating $p_{\rm i}$ up to the flattop time. The ion energy source rate fueled by the centrally peaked NB deposition dominated the establishment of $w_{\rm i}$. This explains why there were no abrupt transitions to supershot conditions (and to Hot-ion H-mode core conditions).

2.5 Electron heating

The dominant electron energy balance can be approximated by

$$p_{\rm e} \equiv p_{\rm be} + p_{\rm ie} + p_{\rm oh} + p_{\alpha e} \simeq \frac{\partial w_{\rm e}}{\partial t} + p_{\rm rad} + p_{\rm e-conv} + p_{\rm e-cond} \tag{3}$$

with $p_{\rm e}$ the effective electron heating rate, $w_{\rm e}$ the electron energy, $p_{\rm oh}$ the Ohmic heating rate, $p_{\rm rad}$ the radiation emission rate, and $p_{\rm e-conv}+p_{\rm e-cond}$ the convected and conducted electron energy flows. TRANSP computes additional terms which have relatively small values for the discharges without IC or electron cyclotron EC heating studied here. Like equation (2), equation (3) is accurate across the whole TRANSP radial domain. The radial profiles of $p_{\rm e}$ are centrally peaked, but not as peaked as those of $p_{\rm i}$. Their profiles are similar to those of $w_{\rm e}$ and T_e.

TRANSP has a run mode where the alpha heating is ignored. With this mode the analysis of DT discharges has the computed $p_{\rm e-cond}$ rate reduced by $p_{\alpha e}$. Below, the electron heating without alpha heating is denoted $p_{\rm e3} \equiv p_{\rm e} - p_{\alpha e}$.

Evolutions of the central $p_{\rm e}$ are shown in figure 5-a),-b). The $p_{\rm be}$ contribution peaks early in the NB phase and rolls over as $n_{\rm e}$ increases. Their values are a factor of 10 lower than $p_{\rm bi}$ shown in figure 4-a), and decrease with isotopic mass from DD to DT. In the DD conditioning series, figure 5-b) they decrease with conditioning in the flattop phase, but increase with conditioning early in the NB as the $n_{\rm e}$ profiles evolve to extreme peaking.

Trajectories of the central $w_{\rm e}$ versus the time-integrated $p_{\rm e}$ are shown in figure 5-c),-d). The linear behavior indicates that $p_{\rm e}$ dominated the establishment of $w_{\rm e}$. The plots versus the time-integrated $p_{\rm e3}$ of the DT supershots without including $p_{\alpha e}$ are rotated clockwise by about 10 %, reducing $p_{\rm e}$ at high $w_{\rm e}$ as seen in figure 2-a). Thus no qualitative difference between the DD and DT supershots are evident.

Trajectories of central $w_{\rm e}$ versus the time-integrated $p_{\rm e}$ with and without $p_{\alpha e}$ are shown for the record $Q_{\rm DT}$ supershot in figure 6-a). Time evolutions of central $w_{\rm e}$ and the time-integrated $p_{\rm e}$ with $p_{\alpha e}$ are shown in figure 6-b). The difference between the time-integrated $p_{\rm e}$ and the lower $w_{\rm e}$ shows the accumulated effects of the convected, conducted, and radiated electron energy losses.

2.6 Summary for TFTR

The low edge density facilitated beam penetration to the center, triggering a synergistic coupling. In both the DD conditioning series with increasing performance with wall conditioning and in the triplet as DD was changed to DT, the central beam - thermal ion heating rate $p_{\rm bi}$, $p_{\rm i}$, and $p_{\rm ie}$ increased at equal times. Central $p_{\rm e}$ increased in both sets. The energy slowing down rate of the full energy beam ions decreased. The total (D and T) beam deposition rate in the center increased, but the beam ion density decreased. The alpha heating contributions to this cycle are relatively small. The beam torque in the center is high in supershots, and increases with decreasing slowing down time. The increased Ω_{tor} could have played a significant role in this cycle. Due to this coupling it is difficult to separate the dominant causes and effects, let alone contributions from smaller causes such as $p_{\alpha e}$.

In this analysis we focused on the heating rates. Alternatively one could compare the heat outflows with $p_{\alpha e}$, but a complication is that although TRANSP knows profiles of the energy conduction and convection we don't have an accurate theory of what they should be or how they change in the presence of alpha heating.

There are reliable radiation emission profiles derived from bolometry measurements. The profiles are similar for DD and DT supershots with low emission in the center, higher near the last closed flux surface. The heating rates from the center of the DT triplet supershots are a factor of three lower than the computed alpha heating rates.

The profiles of $p_{\rm i}$ are high and centrally peaked with shape very similar to those of T_i. The profiles of $p_{\rm e}$ have lower magnitude and peaking, and also are very similar to those of T_e. These similarities suggest that the computed $p_{\rm e}$, with alpha heating is relevant to T_e. The linearity of central T_e and T_i up to the flattop reinforce the notion that T_i is the main driver. The highest T_e is seen in the afterglows following sharp decreases of the central $n_{\rm e}$. Usually they were seen after the CX time window so the T_i and $p_{\rm ie}$ were unknown.

The TRANSP computed energy transport coefficients from the ratios of the energy fluxes and the temperatures gradients. The results for the electron conductivity $\chi_{\rm e}$ computed from $p_{\rm e-cond}$ in the core of the triplets are 0.08-0.10 m^2/s near the time of peak global neutron emission, $S_{\rm n}$. TRANSP simulations were performed turning p_α off in 89402 and increasing T_i by 10%, which is approximately the measurement statistical error. The required $\chi_{\rm e}$ in the core was reduced only slightly, indicating that the computed alpha heating is not required to maintain positive $\chi_{\rm e}$.

We conclude that the likely explanation of high T_e and T_i in the center of supershots both with and without tritium is the synergistic coupling of ion and electron heating. The larger T_e and T_i with tritium could be due simply to enhanced NB deposition in the center.

3. JET alpha heating experiment

3.1 Description of discharges

The JET alpha heating discharges were a set of Hot-ion H-modes with $I_{\rm p}$=3.8 MA and $B_{\rm tor}$=3.6 T. As in TFTR supershots the line-averaged electron density was very low at the start of NB, $\simeq$ 15% of the Greenwald empirical limit and increased to modest ratios $\simeq$ 55% at peak performance. Unlike in TFTR, $n_{\rm e}$ usually increased sharply after the NB phase. Large ELMs occurred late in the NB phase. The mix of D and T was varied by changing the mix in the gas inputs and in the NBI while maintaining their total powers approximately constant ($P_{\rm NB} \simeq$ 10.3MW). Several of these discharges had global fusion power gain $Q_{\rm DT}$ of $\simeq$0.7, and core values $q_{\rm DT}$ above 1.1. These are among the highest values achieved.

Waveforms of one of the highest performing DT discharges in the alpha heating series are shown in figure 7. Summaries of the discharges studied are in table 2. Six of them were the original scan in [3]. The additional ones are the DD 41069 and the DT 42853 and 42855. The TT 43011 in the original scan is not compatible with the others [5], so it is not included in the results that follow.

Sawteeth had an important effect in the peak core temperatures achieved in the alpha heating experiment [5]. Systematic increases in the delays of the occurrences of significant sawteeth with increasing tritium content are seen in the ECE emission near the magnetic axis are shown in figure 8. The ordering of the discharges in this figure and in table 2 is that of the times t_c of the first significant sawteeth. Note that none of these waveforms show afterglows as seen in TFTR figure 1-c). Generally the core $n_{\rm e}$ increased at termination of NB unlike in TFTR.

The TRANSP inputs, modeling, and validity for JET are discussed in Appendix B. The TRANSP modeling was very similar to that used for TFTR. Good agreement with the central and global neutron emission was achieved for all but two discharges in the scan.(41069 and 42847).

Dominant central electron heating rates for one of the representative DT discharges are shown in figure 9-a). These rates are considerably less than those in TFTR (figure 2-a)), which is expected since JET has a much larger volume and smaller auxiliary heating power $P_{\rm aux}$. Most of the discharges in the scan have $p_{\rm ie}$ changing sign near the mid-radius when $T_i \lesssim T_e$. Also T_i is smaller and $p_{\rm ie}$ is a smaller fraction of $p_{\rm e}$. Thus the fraction $f_{\rm alp}$ shown in figure 9-b) and summarized in table 1 is higher. The evolution for the record $Q_{\rm DT}$ discharge 42976 is also shown. It terminated with a"giant ELM' occurring after 13.4 s. It had IC heating so energy balance requires terms added in equations (2) and (3). In the flattop phase $\simeq$14.0 s $p_{\alpha e}$, $p_{\rm be}$, and $p_{\rm ie}$ are comparable. Profiles of the heating terms of a representative DT discharge at a time in the flat-top phase are shown in figure 9-c).

The 2016 reanalysis [5] showed that the alpha heating was not clearly demonstrated, and that isotopic mass scaling was clearly evident. The central temperatures and stored electron energy densities of each discharge at equal times during the rampup phase correlate well with $< A >_{\rm hyd}$ until the discharge experienced a significant sawtooth crash. Soon after the crash T_e recovers a peaked profile and continues to increase with approximately the same rate as before

until the flat-top phase was achieved. Thus the occurrences of these large sawtooth crashes set back the temperatures in the core; the time delay δ_{st} between the last insignificant sawtooth near the start of NB injection and the time t_c of the first large significant sawtooth crashes scaled with $< A >_{\rm hyd}$ and $f_{\rm NBT}$.

As in the center of TFTR supershots, the Equations (2) and Eq. (3) are good approximations for the TRANSP results for the JET alpha heating scan. Radiation emission profiles are not available for these discharges so a coronal equilibrium model in TRANSP was used for a rough estimate of the profiles. The predictions are moderately peaked, unlike the profiles measured in TFTR.

Profiles of $p_{\rm i}$ and $p_{\rm e}$ defined in Eq. 2 and 3 are shown in figure 10. The first at 13.6 s is before any of the discharges experienced a significant sawtooth collapse. The second at 13.75 s, closer to the end of the ramp-up phases when the DD discharges, which had experienced their first significant sawteeth. The last at 14.0 s is during the flattop phase. These times are used for the database studies discussed in the next section, which shows that the peak T_e and T_i increase systematically as $< A >_{\rm hyd}$ (and $f_{\rm NBT}$) increased at the first two times and tend to saturate or decrease at the last time.

The central values of $p_{\rm i}$ and $p_{\rm e}$ show a hierarchy of values with $< A >_{\rm hyd}$ and $< A >_{\rm hyd}$ at all three times. The profiles of $p_{\rm i}$ are more peaked than those of $p_{\rm e}$, as is the case in TFTR. Their shapes are similar to those of the T_i and T_e profiles, also as in the case of TFTR. Profiles of T_i and T_e at two of these times are shown in figure 9 in [5].

The central T_e vs T_i correlate linearly up to the time of peak T_i as shown in figure 11-a) further suggesting that T_i is driving T_e at least up to the flattop phase. This correlation holds even through the significant sawtooth crashes in the DD discharges.

Trajectories of $w_{\rm i}$ versus the time-integrated $p_{\rm i}$ are shown in figure 11-b). Trajectories of $w_{\rm e}$ versus the time-integrated $p_{\rm e}$ are shown in figure 11-c). Evolutions of the central $w_{\rm e}$ and the time-integrated $p_{\rm e}$ are shown in figure 11-d).

The synergistic coupling which occurred in the center of supershots was weaker in the JET Hot-Ion H-modes. One striking difference was that the edge $n_{\rm e}$ tended to increase with increasing tritium in JET. The energy slowing down rate of the full energy D and T beam ions increased with increasing tritium content unlike in supershots. Also their profiles were not centrally peaked as in supershots. The beam-ion density increased. Central $p_{\rm bi}$ and $p_{\rm ie}$ increased at equal times. Central $p_{\rm be}$ increased early in the NB phase, then decreased. The beam torque in the center increased. The increased Ω_{tor} could have played a significant role in this cycle. Due to this coupling it is difficult to separate the dominant causes and effects, let alone contributions from smaller causes such as $p_{\alpha e}$.

The central T_e and T_i at equal times are tightly correlated with $< A >_{\rm hyd}$ and with the delay to the first significant sawteeth at later times. The total fast ion beta toroidal $\beta_{\rm fast}$ and the beam ion beta toroidal β_{bm} are also correlated with these for the shots with moderate $< A >_{\rm hyd}$, but appear to saturate at large $< A >_{\rm hyd}$ ($\gtrsim 2.6$). TRANSP analysis shows that the toroidal beta of the alpha particles is small compared to that of the fast beam ions β_{bm}. TRANSP simulations based on one of the DT discharges with T_e and/or T_i scaled down to DD discharge values have fast ion parameters in qualitative agreement with those in the DD discharges suggesting that high β_{bm} is a consequence, not a direct cause of high T_e and T_i. See figure 12. Values from the simulations are given in table 3.

3.2 Database correlations of T_e and T_i

The 2016 reanalysis is extended to compare additional discharge parameters with the central T_e and T_i. Correlations are shown at three times chosen to separate effects of sawtooth crashes. The first, at 13.6 s before any of the discharges experienced a significant sawtooth collapse are shown in figure 13. figure 13-a) shows the core temperatures tended to increase with the time t_c of the first significant crash (occurring in the future). A plot versus the delay δ_{st} between the last insignificant crash and t_c shown in figure11-a) of [5] has similar trends. figure figure 13-b) shows their correlations with the the central isotopic mass. figure figure 13-c) shows them versus the core fast ion beta $\beta_{\rm fast}$ (the sum of the beam ion beta β_{bm} and the fast alpha beta β_{α}). figure figure 13-d) shows them versus the total neutron emission rate $S_{\rm n}$. The core T_i values tend to increase with t_c, $< A >_{\rm hyd}$, $\beta_{\rm fast}$ and $S_{\rm n}$. Their dependencies on the core fast alpha density n_{α} in figure 13-e) and alpha electron heating rate $p_{\alpha e}$ in figure 13-f) do not show clear scaling. The scalings of T_e are weaker. Power law scalings are shown in the plots.

Correlations at the second time 13.75s after both DD discharges had significant sawtooth crashes are shown in figure 14. An advantage of considering later times is that the discharges are closer to quasi-steady state, and to have had more time for the alphas to slow down, but at later times more discharges experienced significant sawtooth crashes, so there are fewer discharges to compare.

Correlations at 14.0 s are shown in figure 15. By this time the discharges were near flat-top conditions, and only five had not experienced their first significant sawtooth. A least two had signs of distress, for instance roll overs of central T_e as seen in figure 8.

At the first two times the core T_i scales strongly with t_c and scales with $< A >_{\rm hyd}$ approximately as $T_i(0) \propto < A >_{\rm hyd}^{0.6}$. The scaling at 14.0s is much weaker.

No trends, or even contrary trends are seen in figure 15 suggesting T_e saturation around 12 keV at high T_i. If T_e is clamped by some mechanism it would be impossible to prove alpha heating solely on the basis of increased T_e. This could be a hindrance for commercial fusion energy.

This raises the questions of whether the positive scaling seen earlier is a feature only of ramp-up conditions or whether there are too few comparable discharges not limited by MHD.

Both the central and total stored energies at 13.6 s and 13.75 s during the rampup correlate with $< A >_{\rm hyd}$ as shown in figure 16. The scalings seen are compared with other studies in Appendix B.

Although the central temperatures and stored energies correlate well with $< A >_{\rm hyd}$, this does not establish cause. The total heating power was approximately constant, but there were systematic changes in beam parameters as the D and T beam ion mix was changed. For instance, the voltages and penetrations of D and T bean ions differ. The partition of beam heating power to electrons and ions changed. Also the beam ion species and energy densities changed, potentially changing the turbulence drive and stability. The measured toroidal rotation varied, but the Hahm-Burrell flow shearing rate profiles do not show a clear $< A >_{\rm hyd}$ dependence.

The issue of whether $< A >_{\rm hyd}$ or fast ion effects are the cause of enhanced confinement is significant since $< A >_{\rm hyd}$ enhancement would be inherent in DT reactors. Fast ion parameters are expected to be less significant in DT reactors compared with current experiments (due to high densities envisioned for reactors) so their enhancement effects are expected to be small. This raises the question of whether these differences contributed to the higher temperatures and confinement in the DT and TT discharges. The fast ion pressure also varies as the D and T mix was changed.

The comparisons [3, 4] of T_e at the times just before the last significant sawtooth crash instead of at equal times after the start of NBI led to an over-emphasis of the increase of T_e in the DT discharges, and to an over-estimation of $p_{\alpha e}$ effects on T_e and consequently of the need for exotic effects to explain high T_i, such as fast ion stabilization of turbulence and changes in confinement induced by the resonance of alpha particles. Here the scaling is attributed to the thermal hydrogenic mass $< A >_{\rm hyd}$ and / or $f_{\rm NBT}$.

Neither $S_{\rm n}$ nor $p_{\alpha e}$ are linearly correlated with δ_{st} or t_c. This suggests that increasing $< A >_{\rm hyd}$ and/or $\beta_{\rm fast}$ are the causes of longer t_c and δ_{st}, and thus contributing to the higher core T_i and indirectly T_e. The evolutions of various plasma parameters preceding the first significant sawtooth are discussed in Appendix B.

3.3 Summary for JET

The JET alpha heating series had lower ratios of T_i/T_e and thus lower values of $p_{\rm ie}$ and thus larger $f_{\rm alp}$ than TFTR. Significant sawtooth collapses occurring near the end of the rampup phase setback the increasing T_i and T_e. The times of these breaks scaled with $< A >_{\rm hyd}$ and $f_{\rm NBT}$ and thus contributed to the scaling of T_i and T_e with $< A >_{\rm hyd}$ and $f_{\rm NBT}$. Appendix B shows that no unique cause of these sawtooth breaks is evident in the phenomenology. Multiple core parameters start to decrease within a second of the crashes. The DD and TT discharges were not very comparable with the DT discharges leading to ambiguities in separating the causes of their differences. The scaling of T_i and T_e.with the fast ion pressure and with the alpha density or heating rates were also ambiguous.

4. ITER predictions

Numerous predictions for ITER performance have been made. Here we use a new prediction for an ITER ELMy H-mode similar to those discussed in [11, 17–19] with plasma current ramped up to flattop at 15 MA. Negative ion neutral beam injection of 1 MeV D is modeled in TRANSP using NUBEAM. ICRH heating and current drive are modeled with TORIC in TRANSP assuming a He^3 minority with density 2% of n_e. The chosen frequency 52 MHz resonates near the magnetic axis. The ECH/ECCD is modeled using TORAY in TRANSP assuming a frequency of 170 GHz launched from five launchers. Sawtooth effects and slow buildup of the thermalized alpha ash to an equilibrium profile are modeled [17, 18]. We use a pessimistic assumption of an inward pinch for the ash transport and for the fraction of ash recycled in from the scrape-off region

We specify a moderately peaked electron density profile ramped up to 83% of the Greenwald density, shown during the flattop in figure 17-a). The prediction uses GLF23 to predict T_e and T_i shown in figure 17-b). Boundary values are specified to be 5.6keV. Toroidal rotation was computed assuming momentum transport one-half the ion energy transport.

The auxiliary heating power waveforms are assumed to start with the full available power to establish H-mode conditions, and then reducing the power assuming alpha heating and/or hysteresis will maintain the fusion power and maximize $Q_{\rm DT}$. This would resemble the TFTR supershot postlude phase shown in figure 1-a) with the largest $f_{\rm alp}$ shown in figure 2-b). The NB, IC, and EC powers are assumed to start at 33, 20, and 20 MW, then to reduce the IC to 17 MW and the EC to zero after 130s. The global $Q_{\rm DT}$ increases to 7.0 in the $P_{\rm ext}$=50 MW phase. The central $q_{\rm DT}$ is 3 and increases to 8 near the mid-radius.

Many ITER predictions have $T_e > T_i$. The prediction used here has $T_i > T_e$ and thus positive $p_{\rm ie}$ like the TFTR and JET alpha heating plasmas. Results from the ITER prediction in the $P_{\rm aux}$=50 MW postlude phase are given in table 1. The value for $f_{\rm alp}$ is 0.5.

The plasma regimes in TFTR and JET considered here are very different from those in the ELMy H-mode predicted for ITER here. One question concerning the extrapolation of isotopic mass effects to ITER and beyond is to what extent do these effects depend on the presence of fast ion density and energy. The fast ion density fractions in TFTR supershots and JET Hot-ion H-mode discharges were higher than anticipated in ITER. The prediction used here has core values for $n_\alpha/n_e \simeq 0.4\%$ and $\beta_\alpha \simeq 0.6\%$. Comparisons are discussed in [18]. Another question is whether the mass scaling depends on a high ratio T_i/T_e. Also the toroidal rotation Mach number predicted for ITER is low [18] relative to values seen in high performance TFTR and JET discharges. Thus rotation-induced flow shear could be less likely to suppress transport in ITER.

5. Summary and Discussion

New analysis of TFTR supershots and JET alpha heating Hot-ion H-mode discharges presented here used accurate TRANSP simulations of the neutron emission rates suggesting that these runs give accurate predictions of alpha heating. These analysis runs used minimal assumptions and a maximal set of measurements as inputs.

The neutron emission rates are sensitive to the impurity density profiles. Since the only ion densities measured were of trace carbon, an effective impurity was assumed with the shape of the carbon density, but with the charge altered from 6. Good predictions of global and central neutron emission rates were achieved, more accurate than previous analysis using either measured $Z_{\rm eff}$ profiles or single impurity ion densities profiles. Accurate results with variation of the average impurity charge $< Z >_{\rm imp}$ typically have lower $< Z >_{\rm imp}$ early in the NB phase, and sometimes higher than 6 at later times. In TFTR low values of $< Z >_{\rm imp}$ are qualitatively consistent with trace Li from pellet injection wall conditioning. In JET trace Be from the first walls were contributing. Higher values late in the discharges are consistent with contributions from trace concentrations from high Z ions. The choice of $Z_{\rm eff}$ affects the alpha particle source rates. Thus simulations that match the measured DT neutron emission have more credibility predicting the alpha heating rates.

Effects of sawtooth mixing of alpha particles in the JET alpha heating discharges are discussed in [5]. This mixing is predicted to have large effects on the fast ion and alpha heating profiles.

TFTR supershots achieved large alpha heating and electron heating rates, but their $p_{\alpha e}$ was small compared with the measurement and modeling uncertainties. The computed ion to electron energy exchange rate $p_{\rm ie}$ was the largest central electron heating rate in the main NB phase, and the beam-electron heating rate $p_{\rm be}$ was the next highest. Next, the alpha heating and Ohmic heating rates in the center were comparable. This paper gives new results for supershots with late low beam power allowing T_i measurement during low $P_{\rm NB}$. Still the maximum of the alpha to total electron heating rate was less than $f_{\rm alp} \simeq 0.3$ with especially large uncertainty at the largest values. Typical DT supershots had peak rates around 0.2 or less.

An electron power balance analysis for a TFTR supershot was reported in [5]. The discharge studied was the supershot with highest $Q_{\rm DT}$ and had very high T_i/T_e and thus high $p_{\rm ie}$ at the time of maximum $P_{\rm DT}$. Results are included in table 1.

The JET Hot-Ion H-mode discharges had smaller alpha heating and electron heating rates, but their peak ratio $f_{\rm alp}$ was larger than in TFTR, summarized in table 1. The occurrences of sawteeth setback the increasing central T_e which along with other MHD complicated the analysis. The delay to significant sawteeth and the scaling of T_e with the hydrogenic isotopic mass $< A >_{\rm hyd}$ obscured increases in T_e. Also $< A >_{\rm hyd}$ correlated with beam ion parameters, which also effect T_e.

Both experiments had discharge durations too short for the computed alpha heating to equilibrate in flat-top conditions. Both had difficulties producing comparable TT discharges which are pivotal for separating alpha heating from other effects such as the isotopic effect. A problem in TFTR was that D release from the limiter diluted the T, thus limiting $< A >_{\rm hyd}$. A problem for JET was the limited T allowance prevented saturating the first walls with T. Both experiments also had difficulties producing comparable DD discharges. Especially the JET experiment was complicated by the frequent occurrences of transients in the beam power waveforms and by occurrences of significant sawteeth during the flattop phase, both of which effected T_e. Previous interpretation of both experiments suffered from insufficient modeling efforts.

The 2016 reanalysis of the alpha heating experiments in the JET 1997 DTE1 campaign results in significant differences with the early published analysis [3, 4]. The TT discharge used in those papers to conclude the absence of isotopic mass effects is found to be unsuited for inclusion in the scan, due to its high recycling rate. The reanalysis using the other, more comparable TT discharge in the scan shows that at equal times in the discharges, core T_i, T_e, and the total stored energies scale approximately linearly with the average thermal hydrogenic ion mass $< A >_{\rm hyd}$ during the rampup phase. The central $< A >_{\rm hyd}$ is strongly correlated with the increase of the sawtooth delay δ_t, and the delays of significant sawtooth crashes allowed T_e and T_i to obtain higher values. Thus longer δ_t and $p_{\rm ie}$ could explain the higher T_e.

The computed $f_{\rm alp}$ in JET is up to 0.5. Another difference with the previous analysis is that more realistic modeling of sawtooth effects results in lower values for the computed $p_{\alpha e}$. The scaling with $< A >_{\rm hyd}$ is not seen at late times such as 14 s in the flattop phase, but there are too few comparable discharges to know if this means that the beneficial scaling only exists in the rampup phase.

The correlation of T_e with T_i seen in TFTR supershots and in the JET alpha heating discharges in the rampup phase suggest that T_i is the dominant cause of high T_e. Various causes of improved confinement in the ion energy channel are possible including an intrinsic $< A >_{\rm hyd}$ scaling in the thermal plasma, caused possibly by turbulent flow suppression. Another category of possibilities is that differences in the D and T beam depositions are significant. This appears to be the case in TFTR. The beam heating, toque, and fast ion parameters also differ. For instance, deeper penetration of T-beam relative to D-beam neutrals caused more electron and ion core heating in DT. Also loss of fast alphas in the core might be significant.

Another possibility is that the calculations of alpha heating relying on classical slowing down might be incorrect, so the partition of thermal electron ion heating is wrong. Turbulence could cause rapid exchange of fast alpha energy with ions. These have not been explored sufficiently.

The lack of correlation of T_e with T_i during the JET flattop phase could be due to the scarcity of discharges and MHD effects. But if this indicates an intrinsic upper limit to T_e or to the magnitude of its gradient, then alpha heating might not affect T_e, but rather decrease $\chi_{\rm e}$. This could make it even more difficult to separate alpha heating from other causes.

The trends for T_e and T_i to not scale clearly with $p_{\alpha e}$ or $S_{\rm n}$ even during rampup also suggests that $p_{\alpha e}$ is not playing a significant role in T_e, perhaps partly due to systematic changes in confinement or energy loss rates compensating for increased $p_{\alpha e}$. The wider spread of $w_{\rm i}$ relative to $w_{\rm e}$ with $< A >_{\rm hyd}$ contributes to the trend of T_e increasing with $< A >_{\rm hyd}$ due to the thermal ion-electron energy coupling $p_{\rm ie}$.

Various aspects of the analysis and modeling need further study to increase confidence in the simulations. Examples are the alpha heating $p_{\alpha e}$ and $p_{\alpha i}$ and loss terms, for instance effects of MHD on alpha particles. Also the sawtooth model in TRANSP is simplistic and the sawtooth mixing predictions for alpha ions would benefit from further testing.

It is ironic that an early conclusion of the TFTR team was that scaling of T_i with thermal $< A >_{\rm hyd}$ was clear, and an early conclusion of the JET team was that no scaling of T_i with thermal $< A >_{\rm hyd}$ was clear. In hindsight it appears instead that the scaling in TFTR, and possibly in JET, is with the NBI isotopic mass. effects on beam heating.

6. Conclusions and recommendations

Neutral beam central heating was instrumental in the creation of supershots and Hot-ion H-mode discharges. Preferential heating in DT caused higher temperatures. We conclude that the null hypothesis of no alpha heating in either TFTR or JET has a large, but difficult to quantify p-value, the probability of finding the observed or larger results when the null hypothesis is true. However the calculated alpha heating rates appear consistent and plausible with the experimental data.

The NB heating rate in the core was considerably higher for thermal ions than electrons. The ion heating with tritium was higher than with deuterium. The high T_i/T_e played a significant if not the only role in elevating T_e via $p_{\rm ie}$. Additional contributions to the high ratio were discussed: intrinsic thermal mass scaling, and increased confinement caused by fast ion effects. The observation that T_i was higher in tritium early in the NB phase, at least in TFTR suggests that confinement might have been better even in the Ohmic plasma before the presence of fast ion effects, large rotation, and alpha heating. This suggests experiments with brief NB injection of T into Ohmic D plasmas and D into Ohmic T plasmas with careful isotopic mass and CX measurements.

Future DT experiments are planned for JET in 2019-2020 and in ITER after 2034. Alpha heating and isotopic mass experiments in JET would benefit from a more comparable set of discharges, especially including ones with TT NBI. Avoiding sawteeth could improve the reproducibility for comparisons and simplify the modeling. Also this is expected to increase $p_{\alpha e}$ and T_e. Likewise avoiding transient excursions of the NB power waveforms should help, as would long flattop durations. Discharges with the NB power reduced in postludes for CX measurements would be helpful increasing $f_{\rm alp}$ and $Q_{\rm DT}$ and the credibility of the modeling. Measurements such as core hydrogenic ion densities, radiation emission, recycling, and impurity densities are needed for accurate analysis. Separating alpha heating effects from isotopic mass effects are important, especially since isotopic mass enhancements of transport could help make DT fusion energy easier.

Besides having more comparable discharges with comprehensive diagnostic data, it is important to avoid over-reliance on overly simplistic computer codes for analysis, and eagerness to find the expected results.

Appendix A TFTR data, TRANSP analysis, and validation

Parallel TRANSP analysis was used for TFTR and JET to deduce $< A >_{\rm hyd}$, neutron emission, electron heating rates, and fast ion parameters. The TRANSP techniques used are discussed in [5, 11]. The isotopic mass $< A >_{\rm hyd}$ is calculated from species conservation using the beam neutral ionization rates and the wall recycling and gas fueling rates. Their profiles are peaked in radius, and generally decreased in time. See [14].

The accuracy of the TRANSP analysis is checked by comparing simulations with measurements. Examples of comparisons are shown in [11]. The D and T densities are computed from the beam fueling and wall and gas fueling. The fast beam ion densities are computed from the NUBEAM beam package in TRANSP. NUBEAM uses ADAS and multi-step ionization. The edge recycling and gas puff calculations are based on the edge H-alpha emission

measurements.

TRANSP computes the beam and alpha ion distributions using Monte Carlo techniques. TRANSP keeps separate track of the beam ions resulting from the co or counter plasma current NB injectors as well as from the full, half, and third energy neutrals from the injectors. These can be used to define masses for each subset as $2 + n_{nbT}/(n_{nbD}+n_{nbT})$, but the application of these for central heating becomes esoteric. The full energy component ($\simeq$ 110 keV) dominates in the center. Using $f_{\rm NBT}$ is much more accessible.

TFTR data are stored on an archaic computer cluster and thus are not easily accessible, so examples of profiles are shown. Many of the plasma profiles were highly centrally peaked. As usual for supershots, the electron density and ion temperature profiles were sharply peaked, as shown in figure 18. The toroidal rotation velocity shown in figure 18-c) are broader. Statistical error bars for T_c and $v_{\rm vor}$ are about 10%. Systematic errors are harder to qualify and were not archived. An example of potential error arises from determining of the location of the plasma center. TRANSP computes this by solving the Grad-Shafranov equation with the consistent pressure and q profiles. Slight errors between the TRANSP and CX diagnostic grids could cause large increases in the T_c input as indicated by figure 18-b) and thus in the $p_{\rm ie}$ results on axis.

The T_e profile in figure 18-e) is computed in TRANSP from the ECE measurements versus frequency. The T_c profile in figure 18-f) from the input CX data is mapped by TRANSP to the native TRANSP grid x.

To identify causes of the higher T_e in the DT plasmas we calculate the electron heating rates. Modeling details and validation for the TRANSP runs are discussed next. TRANSP analysis runs were done using a maximal set of measurements as inputs. Validation of the runs was done by comparing predictions with measurements.

The deuterium and tritium densities are needed for calculating $p_{\alpha e}$. Normalized carbon densities were derived from the CX data. These were renormalized using a well-calibrated chordal visible bremsstrahlung signal. An effective single-ion impurity charge $< Z >_{\rm imp}$ is needed. If carbon were the only impurity this would be 6.0, but the average is expected to also have contributions from Li and probably trace quantities of other higher Z ions. If $< Z >_{\rm imp}$ is increased, holding $Z_{\rm eff}$ and $n_{\rm e}$ fixed, the impurity charge (but not density) increases so the hydrogenic ion densities decrease. $< Z >_{\rm imp}$ is not experimentally determined so two choices for the time dependence of $< Z >_{\rm imp}$ are shown in figure 19-a). The $< Z >_{\rm imp}$ labeled 'global' was chosen to get an accurate match with the measured global neutron emission $S_{\rm n}$ as shown in figure 19-b). The $< Z >_{\rm imp}$ labeled 'core' was chosen to get an accurate match with the core neutron emission measured by a neutron collimator array [20], shown in figure 19-c). The core simulation results are shown in figure 19-c), -d). A value of 4.5 would result from equal densities of Li and C with the shape measured for C.

Since the CX last data time for the triplet 89402 is 5.375s, T_i is not known subsequently, and is extrapolated by TRANSP (discussed below). The predicted neutron emission rate simulations depend on CX data and thus there is large uncertainty in the $< Z >_{\rm imp}$ fits beyond the data time range, indicated by the shaded region in figure 19-a).

The TRANSP run using the global $< Z >_{\rm imp}$ is too low for the core neutron rate figure 19-e). This suggests that $< Z >_{\rm imp}$ has a profile dependence, peaked on axis, with the core the values and lower further out with the global values shown in figure 19-a). The maximal neutron emission per volume element comes from volume elements near the 1/4 minor radius. The increases of $< Z >_{\rm imp}$ might be a consequence of Li being transported out of the confined plasma region.

Similar degrees of accuracy have been achieved modeling other supershots using the same method of adjusting $< Z >_{\rm imp}$. Apparently this is the case for all supershots (without high or contorted q profiles). The TRANSP modeling indicates that for both DD and DT supershots $< Z >_{\rm imp}$ increased in time (at least during the NB phases) unless interrupted by disruptions or MHD. This explains difficulties previously seen in modeling $S_{\rm n}$. The DT supershots also appear to have $< Z >_{\rm imp}$ peaked on axis. It is not clear if the same is true for DD supershots since there are no data for their core neuron emission rates. Similarly secular increase of $< Z >_{\rm imp}$ are inferred for the JET alpha heating discharges, but with less or no peaking implied by comparing the global and core DT neutron emission rates.

Variation of $< Z >_{\rm imp}$ might not be the whole story for accurate simulation of neutron emission. There are additional ambiguities in the modeling. For instance the separate thermal D and T densities $n_{\rm D}$ and $n_{\rm T}$ are needed to compute the neutron emission rates. TRANSP computes the total hydrogenic ion density $n_{\rm i} \equiv n_{\rm H}+n_{\rm D}+n_{\rm T}$ by the measured $n_{\rm e}$, $Z_{\rm eff}$, $< Z >_{\rm imp}$, or impurity density profiles and the computed fast ion densities. TRANSP computed

$n_{\rm i}$ and its radial flow from charge conservation. TRANSP has models for computing the separate thermal hydrogenic ion densities and flows with additional assumptions. Some turbulence models predict different transport of different hydrogenic ions [21–25].

Results for $p_{\alpha e}$ and other electron heating rates are shown in figure 2. The alpha heating of ions is computed to typically be about 20% of $p_{\rm e}$.

The CX data for the discharges with beam blips does not exist between the termination of the main NB phase and the blips. TRANSP was used to extrapolate T_i with the simple assumption that the ion heat conduction $\chi_{\rm i}$ is a multiple of the Chang-Hinton prediction. Approximate agreement with the prediction and measurements of T_i in the core at the blips was achieved setting the multiplier to be 25 for the DD discharge and 7.5 for the DT discharge. The different multipliers are qualitatively consistent with the improved ion energy confinement seen in DT. However the Chang-Hinton predicted T_i profiles are considerably broader than measured. In the following, modeling results are used only in temporal regions with CX data.

Additional verification tests include comparisons of the TRANSP-predicted surface voltage, stored energy, and diamagnetic flux. The triplet simulations have $\simeq$15% more stored energy and less surface voltage than deduced from magnets measurements. The choice of restistivity model effects the TRANSP predicted Ohmic heating rate in the center.

Appendix B JET TRANSP analysis, validation, and scalings

The TRANSP analysis was very similar for JET and TFTR. The accuracy of the TRANSP analysis is checked by comparing simulations with measurements. For the alpha heating discharges the trace carbon density was measured. The ratio in the core of the carbon to hydrogenic ion densities for the nine discharges in table 2 was 1-2% up to 14.0s, then increased. The ratio outside the core was larger. For some subsequent Hot-ion H-mode discharges there are measurements of one or more additional trace impurities. As for TFTR, values of $< Z >_{\rm imp}$ were adjusted to match the neutron emission rates. Unlike for TFTR, the values that matched the global $S_{\rm n}$ were close to those that matched the central neutron emission rates measured by the neutron camera. They increased in time from values typically around 4 or 5 to to around 7 or 8. Good agreements were achieved for seven of the nine discharges.

The results for $< A >_{\rm hyd}$ are relatively flat in radius and constant in time, unlike in TFTR. Values at one time are shown in table 2. In the core $< A >_{\rm hyd}$ is dominated by the beam neutral ionization rates, so across the scan the central $< A >_{\rm hyd} \simeq f_{\rm NBT} + 2$. Examples of comparisons are shown in [5]. The time delay to the first significant sawteeth increases with increasing T beam power.

The core T_i and T_e for both the DD and DT discharges were less than typically seen in TFTR supershots. Values of $p_{\rm ie}$ were less than the TFTR values shown in figure 1-d by a factor of two. The core $p_{\alpha e}$ computed by TRANSP shown in figure 9 are considerably higher than the TFTR values shown in figure 1-(d).

Sawteeth play an important role in the peak core temperatures achieved in the alpha heating experiment [5]. The delay of the onset of significant sawteeth in the alpha heating discharges was studied in [26]. Increased beam pressure due to longer beam slowing down times and higher beam densities, and isotope mass effects were identified. Examples of central plasma parameters are shown in figure figure 20 versus time bases which are shifted to align the times of the first significant sawtooth crashes. The DT discharge 42855 is not shown since the first significant sawtooth occurred after the NB when CX diagnostic data is not available. The central $n_{\rm e}$ and impurity density increased throughout the discharges and increased with $< A >_{\rm hyd}$ approaching the crash times. The core parameters for most of the discharges decreased during the last 100 msec preceding the crash time. For instance, the beam densities and beta decrease to the time of first significant sawteeth (as the electron density was increasing) suggesting that high values are needed for sawtooth suppression. The alpha beta increases, but their values are relatively small. The values of β_{bm} needed to suppress sawteeth was higher at higher $< A >_{\rm hyd}$ as shown in figures figure 20-e),-f). This could be due to the higher core temperatures correlated with high $< A >_{\rm hyd}$, as shown in figure 13-b), figure 14-b). The fact that many plasma parameters decrease shortly before the sawtooth crashes indicates that identifying a sole cause of the crashes is challenging.

The delay of the occurrences of significant sawtooth crashes increases with fast ion parameters such as beta. The

isotopic mass and the fast ion beta are correlated. TRANSP analysis shows that the beta of the alpha particles is small compared to that of beam ions. The time delay δ_{st} between the last insignificant crash and the first significant crash is another important parameter. Values of δ_{st} in table 2 tend to increase with $f_{\rm NBT}$ and $< A >_{\rm hyd}(0)$ as shown in figure 11-a) of Ref [5]. Their total increases with increasing isotopic mass, then saturates.

The scaling of core T_e and T_i are shown in figures 13,14,15. The trends for T_e and T_i to increase with t_c, $< A >_{\rm hyd}$, and $\beta_{\rm fast}$, and were strongest at 13.75 s and weak by the flattop time 14.0 s. Too few comparable discharges are available for reliable comparison, especially at flat-top times.

The total stored energy scaling in figure. 16-b) and -d) is $W_{\rm tot} \propto < A >_{\rm hyd}^{0.45}$ at 13.6 s and $\propto < A >_{\rm hyd}^{0.70}$ at 13.75 s. These scalings bracket the scaling of the TFTR supershots.

Scaling of energy transport profiles in JET ELMy H-mode discharge from the DT campaign have been published [27] using local dimensionless parameters: average thermal ion gyro-radius ρ_* and collisionality ν_* normalized by a system scale length, normalized pressure β, and $< A >_{\rm hyd}$. Results for discharges with H, D, or DT in the region $0.3 < x < 0.7$ yielded fits for the ion energy transport $1/\chi_{\rm i} \propto < A >_{\rm hyd}^{0.84\pm0.06}$; the total (convected and conducted) ion energy transport $1/\chi_{\rm i-tot} \propto < A >_{\rm hyd}^{1.06\pm0.06}$; and for the total ion and electron energy transport $1/\chi_{\rm eff} \propto < A >_{\rm hyd}^{0.94\pm0.06}$.

Fits using globally-defined (scalar) dimensionless scaling parameters and local $< A >_{\rm hyd}$ taken from the hydrogenic alpha emission (dominated by the edge) are in [27] The scalings for the thermal energy confinement in ELM-free H modes is $\tau_E \propto < A >_{\rm hyd}^{-0.25\pm0.22}$, and in ELMy H modes: $\tau_E \propto < A >_{\rm hyd}^{-0.03\pm0.10}$. Local transport analysis of five ELMy H mode plasmas from a dimensionless parameter scaling study of DT plasmas were also presented in [28]. The TT discharge was not well matched, as in this present study. The results gave confinement in the edge region increasing strongly with the isotope mass, whereas the confinement in the core region decreases as $\tau_E \propto < A >_{\rm hyd}^{-0.16}$. In the present study $< A >_{\rm hyd}$ in the core is calculated from species conservation using the NBI and recycling sources using TRANSP, discussed above.

Both the central and total stored energies at the first two times correlate with $< A >_{\rm hyd}$ as shown in figure 16. The $< A >_{\rm hyd}$ scaling of JET ELMy H-modes (including DT) were studied in [28]. The energy content was separated into a pedestal and a "confinement region' above the pedestal. The energy stored in the pedestal showed a strong, near linear scaling with $< A >_{\rm hyd}$. A weak or no scaling of the energy in confinement region was found and the paper concluded a very weak scaling of their total. Here, for the Hot-ion H-mode discharges in the alpha heating scan the temperature and density pedestals do not show a clear linear scaling in $< A >_{\rm hyd}$.

The third time, 14s was after the DT discharge with lowest $f_{\rm NBT}$ had its first significant sawtooth crash. An advantage of later times is that the discharges are closer to quasi-steady state, and to have had more time for the alphas to slow down, but at later times more discharges experienced significant sawtooth crashes, so there are fewer un-crashed discharges to compare. Also, by 14.0s at least the discharge 42856 was experiencing n=1 MHD. Some of the others such as 42853 and 42855 experienced roll-over in T_e shown in figure 8.

This work has been carried out within the framework of the EUROfusion Consortium, and has received funding from the Euratom research and training programme 2014-2018 under grant agreement No 633053. The views and opinions expressed herein do not necessarily reflect those of the European Commission. The computer facilities used for this work were supported in part by the US DoE contract No. DE-ACO2-76-09CHO11466. The authors wish to thank the TFTR team, the TRANSP team, R. Bell, M. Gorelenkova, K. Hill, D. Mansfield, S. Scott, G. Taylor, H. Weisen, X. Yuan, M. Zarnstorff, and S. Zweben.

*E-mail: budny@princeton.edu

[a]See author list of [29].

[1] R.J.Hawryluk, H.Adler, P.Ailing, C.Ancher, H.Anderson, *et al.,* Phys. Review Lett. **72** 3530 (1994) http://dx.doi.org/10.1103/PhysRevLett.72.3530

[2] G.Taylor, J.D.Strachan, R.V.Budny, and D.R.Ernst, Phys. Review Lett. **76** 2722 (1996).

[3] P.R. Thomas, P Andrew, B.Balet, D.Bartlett, J.Bull, B.deEsch, *et al.,* Phys. Review Lett. **80** 5548 (1998)

[4] S.E. Sharapov, L.-G. Eriksson, A. Fasoli, G. Gorini, *et al.,* Fusion Science Technol, **53** (2008) 989

[5] R.V.Budny, Nucl. Fusion **56** 036013 (2016)

[6] D. Testa and M. Albergante, Nucl. Fusion **52** 083010 (2012) doi:10.1088/0029-5515/52/8/083010

[7] M. Murakami, J.D. Callen and L.A. Berry Nuclear Fusion, (1976) **16** 347

[8] M. Greenwald, Plasma Phys. Control. Fusion (2002) **44** R27

[9] R.V. Budny, Physics of Plasmas, **18** (2011) 092506 https://doi.org/10.1063/1.3626541

[10] K. Hill, private communication 2017

[11] R.V. Budny, J.G. Cordey, Nucl. Fusion **56** 056002 (2016)

[12] G. Taylor, private communication 2017

[13] Budny R.V., Bell M.G., Biglari H., Bitter M. *et al.,* Nucl. Fusion, **32** (1992) 429.

[14] R.V. Budny, M.G. Bell, D.K.M Mansfield, J.D. Strachan, S. Zweben, *et al.,* 21^{st} EPS, Montpelier, France (1994), available at http:w3.pppl.gov/~budny/PDF/Budny_EuropeanPhysicalSociety_1994.pdf

[15] S.D.Scott, D.R.Ernst, M.Murakami, H.Adler, M.G.Bell, R.Bell, R.V.Budny, *et al.,* Physica Scripta, **51** (1995) 394 doi:10.1088/0031-8949/51/3/021

[16] S.D.Scott, M.C.Zarnstorff, Cris W.Barnes, *et al.,* Physics of Plasmas, **2** (1995) 2299

[17] R.V.Budny, R.Andre, G.Bateman, F.Halpern, C.E.Kessel, A.Kritz, and D.McCune Nucl. Fusion **48**, (2008) 075005

[18] Budny R.V., Nucl. Fusion **49**, (2009) 085008.

[19] Budny R.V., Nucl. Fusion **52**, (2012) 013001

[20] A.L. Roquemore, M. Bitter, L.C. Johnson, and S. von Goeler, Rev. Sci. Instrum. (1997) **68** 544 doi: 10.1063/1.1147648

[21] W.W.Lee and R.A.Santoro Physics of Plasmas **4** 169 (1997)

[22] T.S. Hahm, Lu Wang, W.X. Wang, E.S. Yoon and F.X. Duthoit, Nucl. Fusion **53** (2013) 072002 doi:10.1088/0029-5515/53/7/072002

[23] A. Bustos, A. Banon Navarro, T. Gorler, F. Jenko, and C. Hidalgo, Phys. of Plasmas **22** 012305 (2015) http://dx.doi.org/10.1063/1.4905637

[24] M.Nakata, M.Nunami, and H.Sugama, Phys. Rev. Letters **118** 165002 (2017) DOI10.1103/PhysRevLett.118.165002

[25] S. Buller, I. Pusztai, S.L. Newton, J.T. Omotani Plasma Phys. Cont. Fusion (2017) **59** 055019

[26] M.F.F.Nave, N.N.Gorelenkov, K.G.McClements, S.J.Allfrey, *et al.,* Nucl. Fusion **42** 281 (2001) doi:10.1088/0029-5515/42/3/308

[27] R.V.Budny, D.R.Ernst, T.S.Hahm, D.C.McCune, J.G.Cordey, *et al.,* Phys of Plasmas, **7** 5038 (2000) doi: 10.1063/1.1320466

[28] J.G. Cordey, B. Balet, D.V. Bartlett, R.V.Budny, *et al.,* Nucl. Fusion **39** 301 (1999)

doi:10.1088/0029-5515/39/3/301

[29] Litaudon X., *et al.,* Nuclear Fusion **57** (2017) 102001

discharge	mode	$f_{\rm Gw}$	$Q_{\rm DT}$	$q_{\rm DT}$	$p_{\alpha e}$ MW/m^3	f_{alp}	time sec
TFTR 89402	supershot	25	0.18	0.4	0.053	0.16	5.37
TFTR 89405	supershot	19	0.17	0.4	0.059	0.31	5.37
TFTR 80539	supershot	46	0.28	0.8	0.270	0.14	3.77
TFTR 80539	supershot	53	0.28	0.8	0.300	0.30	3.79
JET 42856	Hot-ion H-mode	34	0.68	1.1	0.042	0.48	14.5
JET 42847	Hot-ion H-mode	34	0.58	1.0	0.040	0.55	14.3
JET 42976	Hot-ion H-mode	32	0.68	1.2	0.060	0.31	13.3
JET 42982	ELMy H-mode	48	0.22	0.7	0.026	0.22	16.4
ITER 20105	ELMy H-mode	86	7	3-8	0.30	0.5	185

TABLE I: *Summary of fusion parameters for the two TFTR DT discharges from the TFTR triplet studied here compared with the TFTR supershot (80539) with record $Q_{\rm DT}$, the JET Hot-Ion H-mode (42976), the ELMy H-mode (42982) with record $Q_{\rm DT}$'s, two of the alpha heating Hot-Ion H-mode discharges studied here, and for predictions for an ITER ELMy H-mode discharge. The record TFTR supershot results are given at two times: first before a minor disruption and second at peak during the "carbon bloom' that rapidly slowed the alpha ions. The ratio $f_{\rm Gw}$ of the line-averaged $n_{\rm e}$ to the empirical density limit, the global $Q_{\rm DT}$, and central values $q_{\rm DT}$ of the profiles are listed. Values of the central alpha-electron heating rate density and it's ratio to the central total (ion-electron $p_{\rm ie}$, beam-electron $p_{\rm be}$ and Ohmic $p_{\rm oh}$) heating rate densities at the times shown. The ratios increase during the discharges and listed at times within the windows of CX data and before disruptions. In equilibrium $f_{alp} \rightarrow q_{\rm DT}/5$. The record fusion power TFTR and JET and an ITER prediction are discussed in* [11].

Discharge	t_c [s]	δ_{st} [s]	$f_{\rm NBT}$	$f_{\rm NBT}$	$\beta_{bm}(0)$ %	$\beta_\alpha(0)$ %	$\beta_{\rm fast}(0)$ %	$< A >_{\rm hyd}(0)$	$p_{\alpha e}(0)$	$n_\alpha(0)$	Exceptions
40365	13.6638	0.9026	0.0	0.0	0.440	0.000	0.43	1.99	0.0	0.0	a,b
41069	13.6849	1.0492	0.0	0.0	0.360	0.000	0.38	1.99	0.0	0.0	a,b,c
42870	13.7987	0.9515	0.27	0.27	0.440	0.079	0.55	2.23	2.1	0.30	
42856	14.1242	1.4565	0.52	0.58	0.780	0.288	1.07	2.55	5.1	1.07	
42855	14.2657	1.2515	0.53	0.60	0.772	0.260	1.05	2.56	4.4	0.90	d
42847	14.3087	1.4015	0.72	0.72	0.820	0.244	1.06	2.70	3.7	0.87	e,f
42853	14.3342	1.1820	0.53	0.63	0.759	0.239	0.98	2.60	4.5	0.89	g
42840	14.3387	1.6100	1.00	0.86	0.900	0.140	0.94	2.79	2.2	0.50	
43011	14.3972	1.6217	1.00	0.98	0.838	0.045	0.88	2.93	0.8	0.20	b,h

TABLE II: *Hot-ion H-mode alpha heating discharges with similar $P_{\rm NB}$, $I_{\rm p}$, and $B_{\rm tor}$ ranked by increasing time t_c of the occurrences of the first significant sawtooth crash (as indicated in figure 8); time delay between the last insignificant and 1st significant sawtooth crash at time δ_t; fraction T beam to total beam power $f_{\rm NBT}$; T alpha line emission fraction in the hydrogenic wall recycling $f_{\rm NBT}$; core beta toroidal of the beam β_{bm}, alpha ions β_α, and their total $\beta_{\rm fast}$; core hydrogenic isotopic mass $< A >_{\rm hyd}$; and the maximum values of alpha parameters in the time window 14.0-14.1s (near the times of maximum $S_{\rm n}$): alpha electron heating $p_{\alpha e}$ [$10^{-2} MW/m^3$]; and number of fast alpha ions [$10^{17}/m^3$]. The values of δ_t, $f_{\rm NBT}$, $f_{\rm NBT}$, and β_{bm}, $\beta_{\rm fast}$, and $< A >_{\rm hyd}(0)$ increase approximately with t_c. The values of β_α, $p_{\alpha e}(0)$, and $n_\alpha(0)$ do not correlate as well with t_c. Note that $< A >_{\rm hyd}(0)$ and $f_{\rm NBT}$ are related as in Eq. 1. Discharges with exceptions (relatively large deviations from the average values): a=low $I_{\rm p}$; b=low core toroidal rotation; c=low $P_{\rm NB}$; d=NBI ended early (at 14.0s); e=high $P_{\rm NB}$; f=mode lock, disruption; g=long-duration NBI, $n_{\rm e}$ increased to 0.8 × $\overline{n}_{\rm Gw}$ with n=1 and 2 MHD 14.2-14.5s, a second peak in $S_{\rm n}$ and high $p_\alpha(0)$ at end of NBI; h=high edge $n_{\rm c}$ and edge recycling. Discharge 43011 is too dissimilar from the others, and is not used for the scaling fits and plots. A similar table (without 42853) is in* [5].

Variable	42856Z11	42856P09	42856P10	42856Z11	42870Z12
T_e/T_i scaled	1.0/1.0	0.955/1.0	1.0/0.862	0.955/0.862	1.0/1.0
$S_{\rm n}$ [$10^{18}/s$]	1.94	1.94	1.62	1.62	1.28
n_α [$10^{16}/m^3$]	8.00	8.00	7.05	6.80	4.60
$\beta_{toroidal}$	0.035	0.035	0.033	0.033	0.031
β_{bm}	0.008	0.008	0.008	0.008	0.006
β_α	0.003	0.003	0.003	0.003	0.002
$p_{\rm bi}$ [MW/m^3]	0.225	0.225	0.225	0.225	0.190
$p_{\rm th}$ [MW/m^3]	0.100	0.100	0.085	0.078	0.070
$p_{\rm be}$ [MW/m^3]	0.035	0.035	0.035	0.035	0.030
$p_{\alpha e}$ [MW/m^3]	0.038	0.038	0.032	0.032	0.025

TABLE III: *Comparison of the global neutron emission rates and central fast ion parameters at 13.75s from TRANSP runs for the the DT discharges 42856 with $< A >_{\rm hyd}$=2.55 with the electron and ion temperatures scaled down by 0.955 and 0.862 to match those of 42870 with $< A >_{\rm hyd}$=2.23. The time is before the first significant sawtooth of either.*

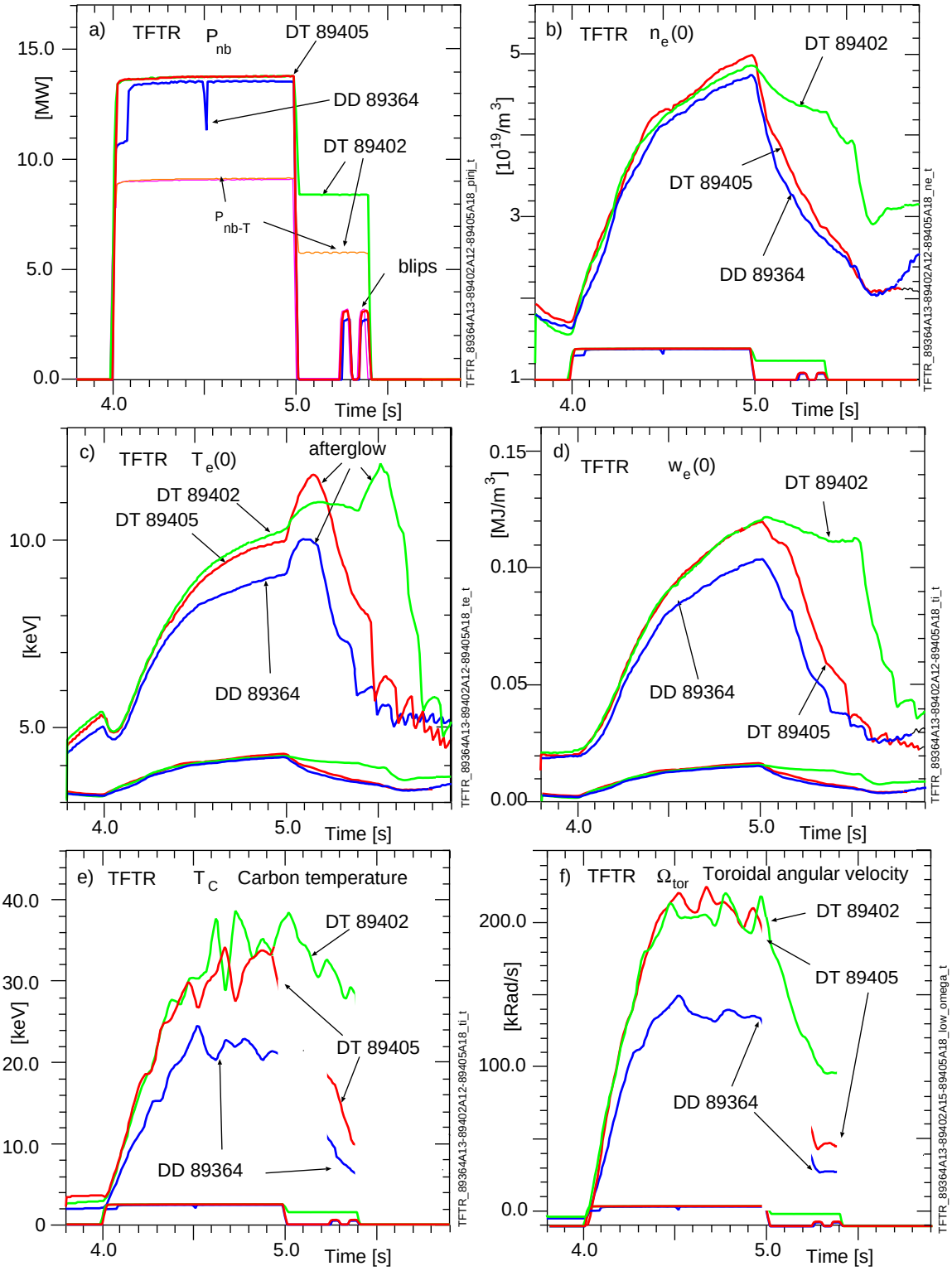

FIG. 1: Waveforms for a well-matched TFTR triplet consisting of one DD and two DT supershots: a) total beam heating powers $P_{\rm nb}$. The DD and one of the DT supershots had two late brief power blips for CX measurements. The NB power in the DT blip supershot was from T-NB. The other DT supershot had a "postlude' with NB power decreased to 60%. The T-NB power for the postlude supershot is indicated; Relatively few DT supershots had late beam blips or postludes; b) central electron density including a schematic of $P_{\rm nb}$; c) central electron temperature from electron cyclotron measurements including a a schematic of $n_{\rm e}$. Sawteeth crashes are seen after the $P_{\rm nb}$ phase. Both the DD and DT show large increases in $T_e(0)$ dubbed "afterglows' when $n_{\rm e}(0)$ decreased. These afterglows were often seen when the central T_e was large and the NB power was turned off. Multiple afterglows such as seen in 89402 were unusual. There have been suggestions that this higher "afterglow' indicates alpha heating. d) central electron stored energy density; e) central carbon temperature; and f) central carbon toroidal rotation velocity. The CX data in the blips were averaged to one time point per blip. The plasma current was constant (2.28 MA) from 4 to 5.5 s, and then was ramped down as the discharges terminated.

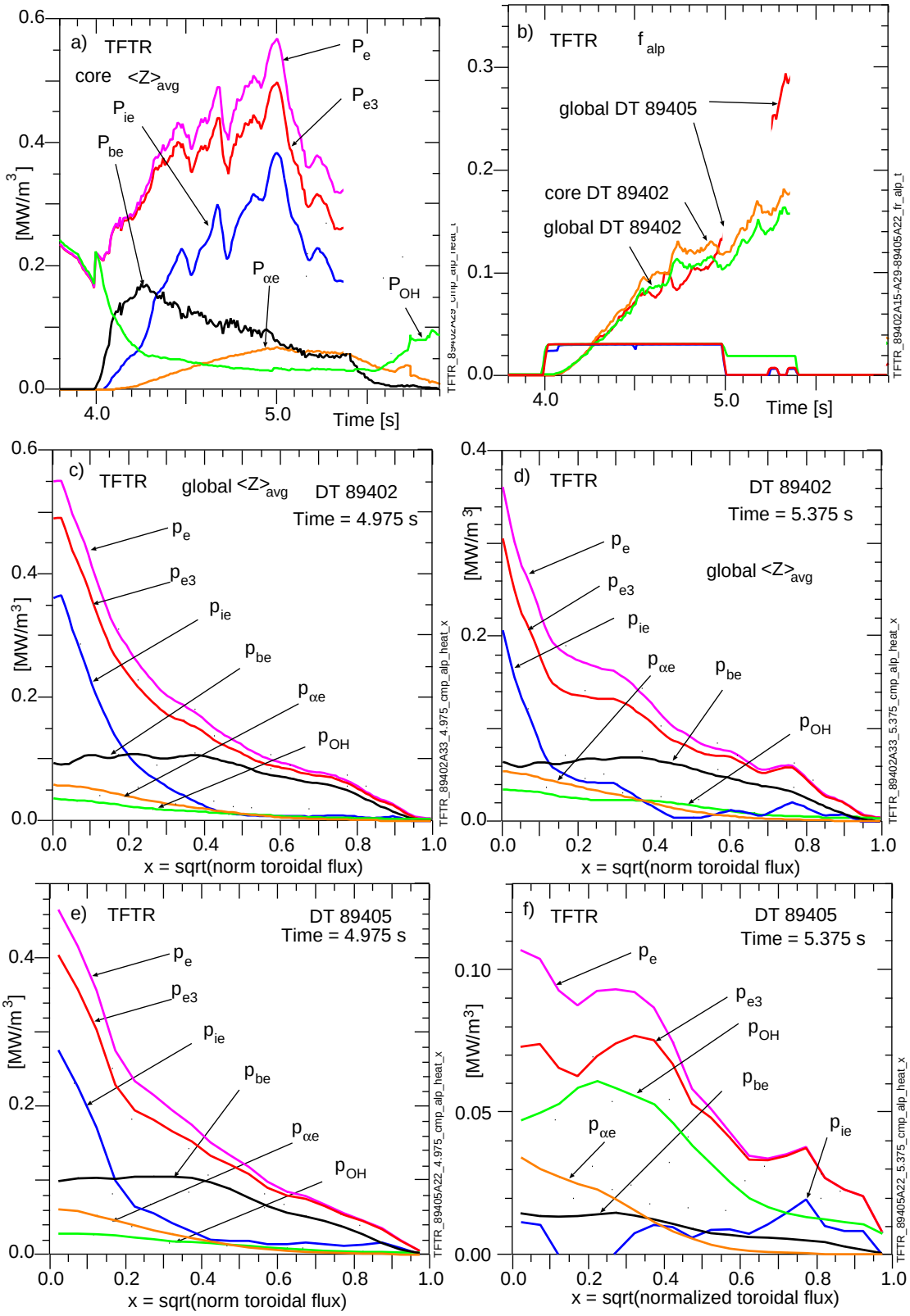

FIG. 2: Electron heating rates: a) time-evolution of the central rates in the DT supershot 89402 with the NB postlude; b) ratio of central $p_{\alpha e}$ and the central effective total electron heating rate p_e for the two DT discharges of the triplet. Global and core choices for $< Z >_{\rm imp}$ (discussed in Appendix A) give similar predictions for $f_{\rm alp}$. The prediction for 89405 at the blip beam blip is the highest $f_{\rm alp}$ predicted for TFTR, due to the low effective total electron heating rate; c) profiles of the rates for 89402 at 4.975 s (near peak) and d) 5.375 s (last time of CX data). e) profiles of the rates for 89405 at 4.975 s (near peak) and f) 5.375 s (last time of CX data). $p_{e3} \equiv p_e - p_{\alpha e}$

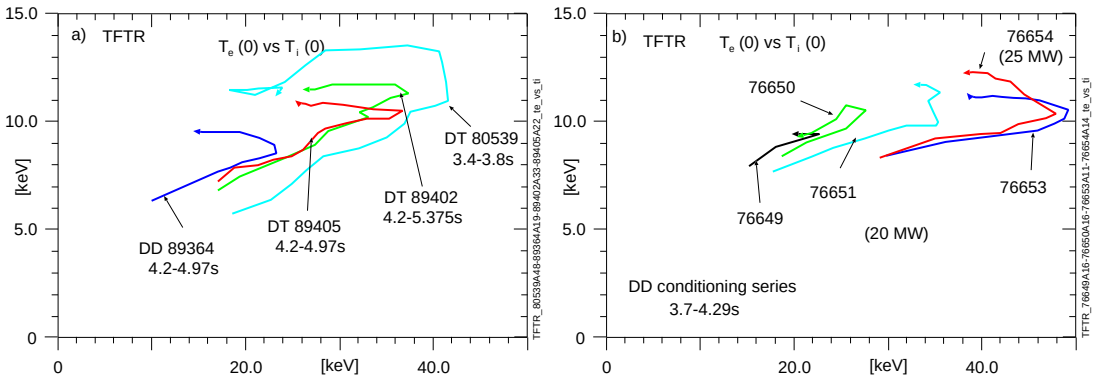

FIG. 3: Trajectories of central T_e vs T_i for a) the triplet and the record TFTR $Q_{\rm DT}$ supershot; and b) the DD supershot conditioning series. The last discharge of the series had $P_{\rm nb}$=25MW. The curves were smoothed. The trajectories have a counter-clockwise direction due to earlier peaking of of T_i relative to T_e.

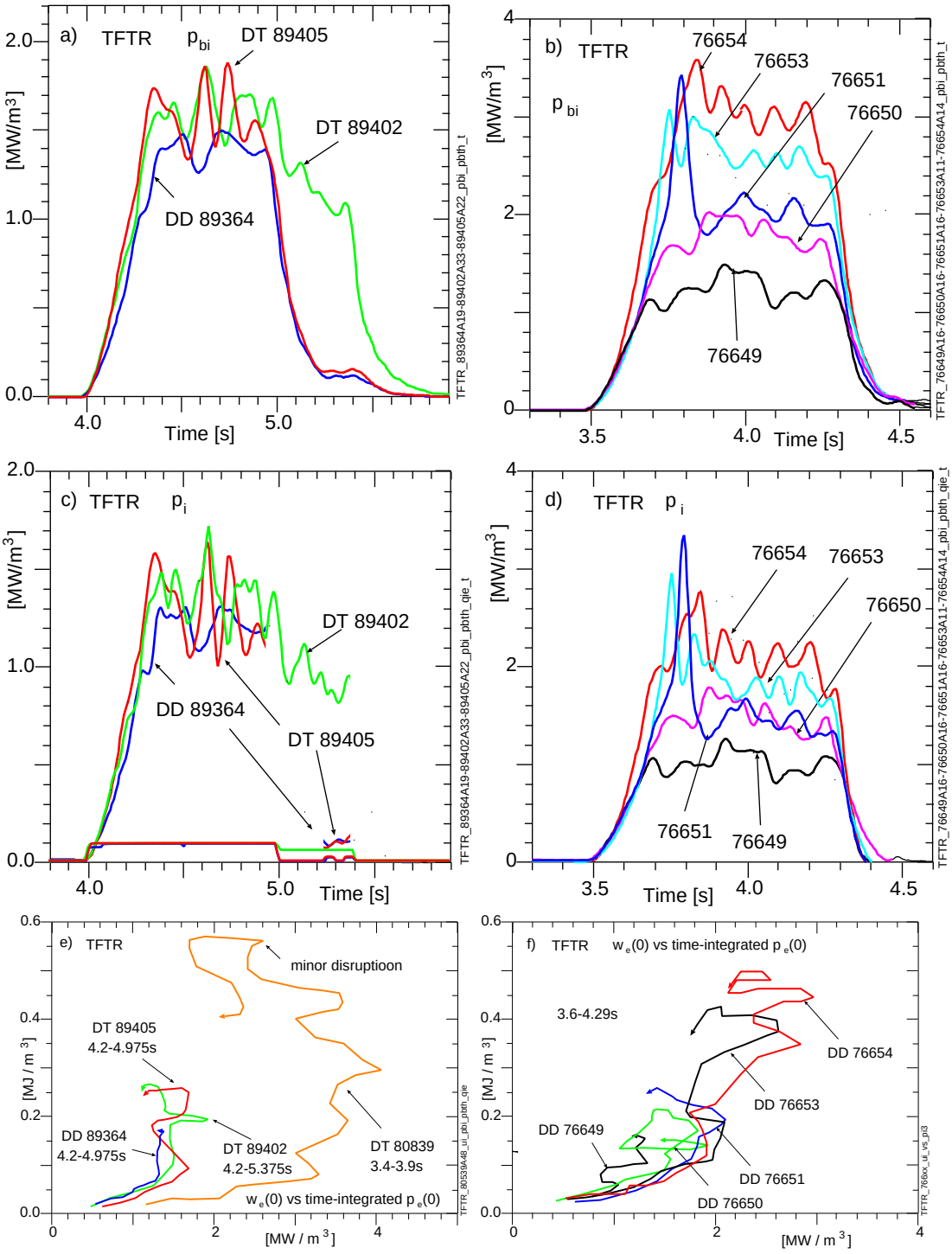

FIG. 4: Evolutions of the central beam-thermal ion heating rates in the a) triplet; b) DD conditioning series. Slight isotopic mass enhancements and large conditioning enhancements are seen. Evolutions of $p_{\rm i} \equiv p_{\rm bi} - p_{\rm ie}$ for the c) triplet; d) DD conditioning series; trajectories of the central thermal ion energy density $w_{\rm i}$ vs the time-integral of $p_{\rm i}$ for the e) triplet and the record $Q_{\rm DT}$ supershot; and f) DD conditioning series. The increases of central $p_{\rm i}$ with conditioning shown in d) correlate with decreases of $n_{\rm e}$ near the edge and increases in the center [9].

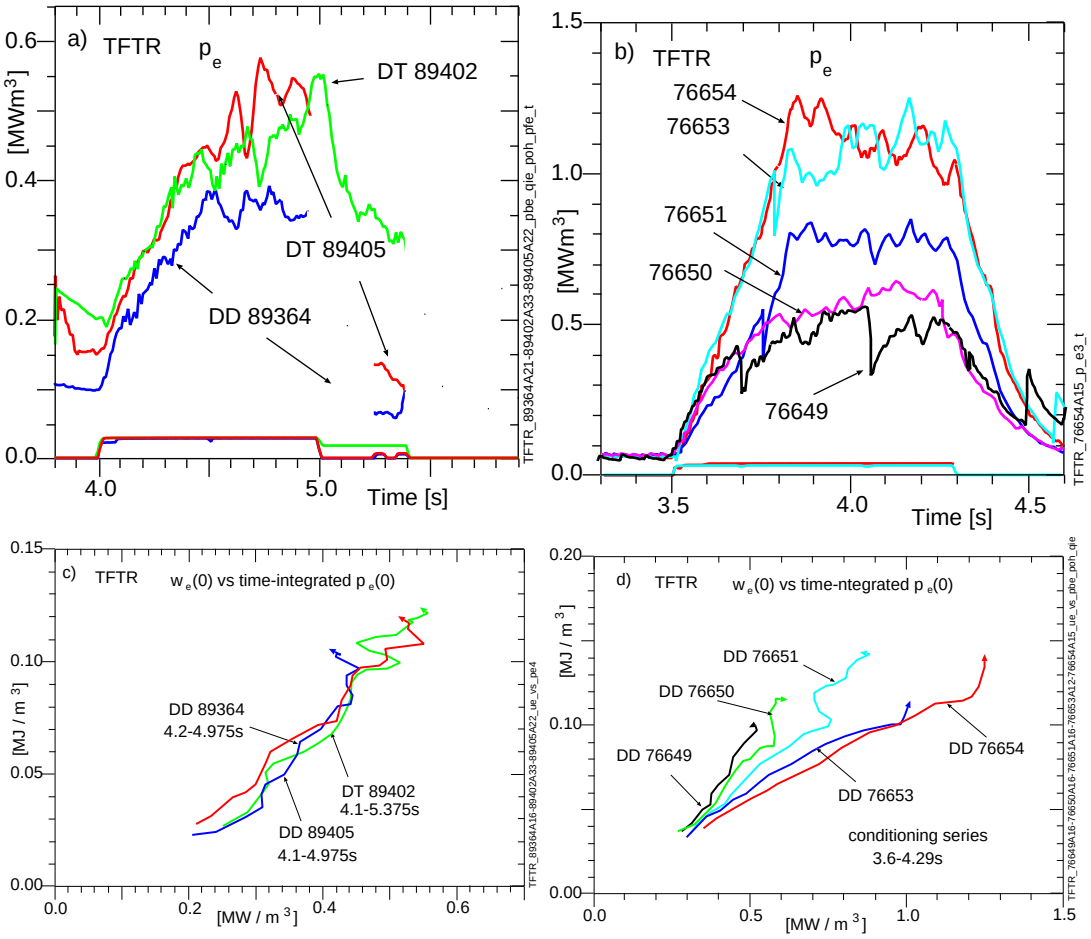

FIG. 5: Evolutions of the three central electron heating rates (including alpha heating) p_{e3} in the a) triplet; b) DD conditioning series; trajectories of the central T_e vs the time-integral of the four central heating rates $p_e = p_{be} - p_{ie} + p_{oh} + p_{\alpha e}$ in the c) triplet; d) DD conditioning series with P_{NB}=19.5-25 MW (and negligible alpha heating).

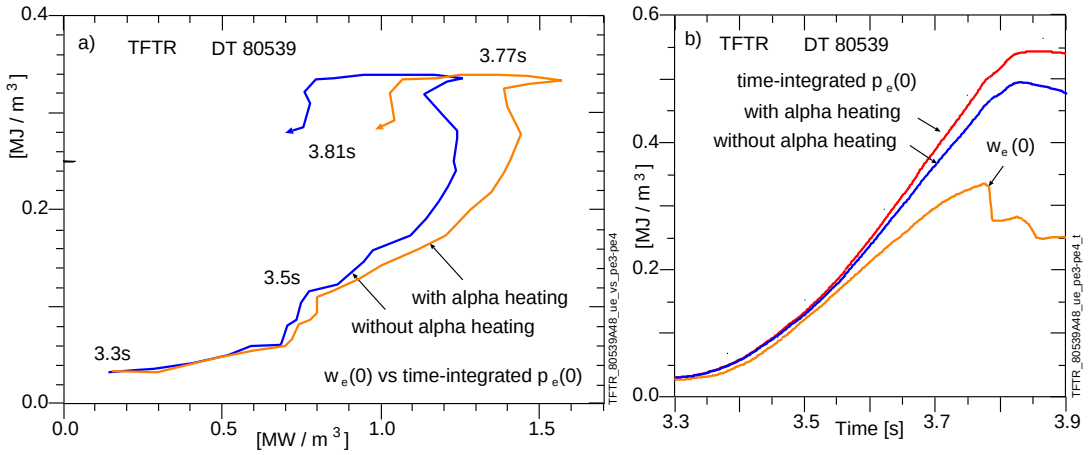

FIG. 6: a) trajectory of central T_e vs p_e with alpha heating in the record Q_{DT} supershot b) comparison of central w_e with the time-integrated p_e with and without alpha heating.

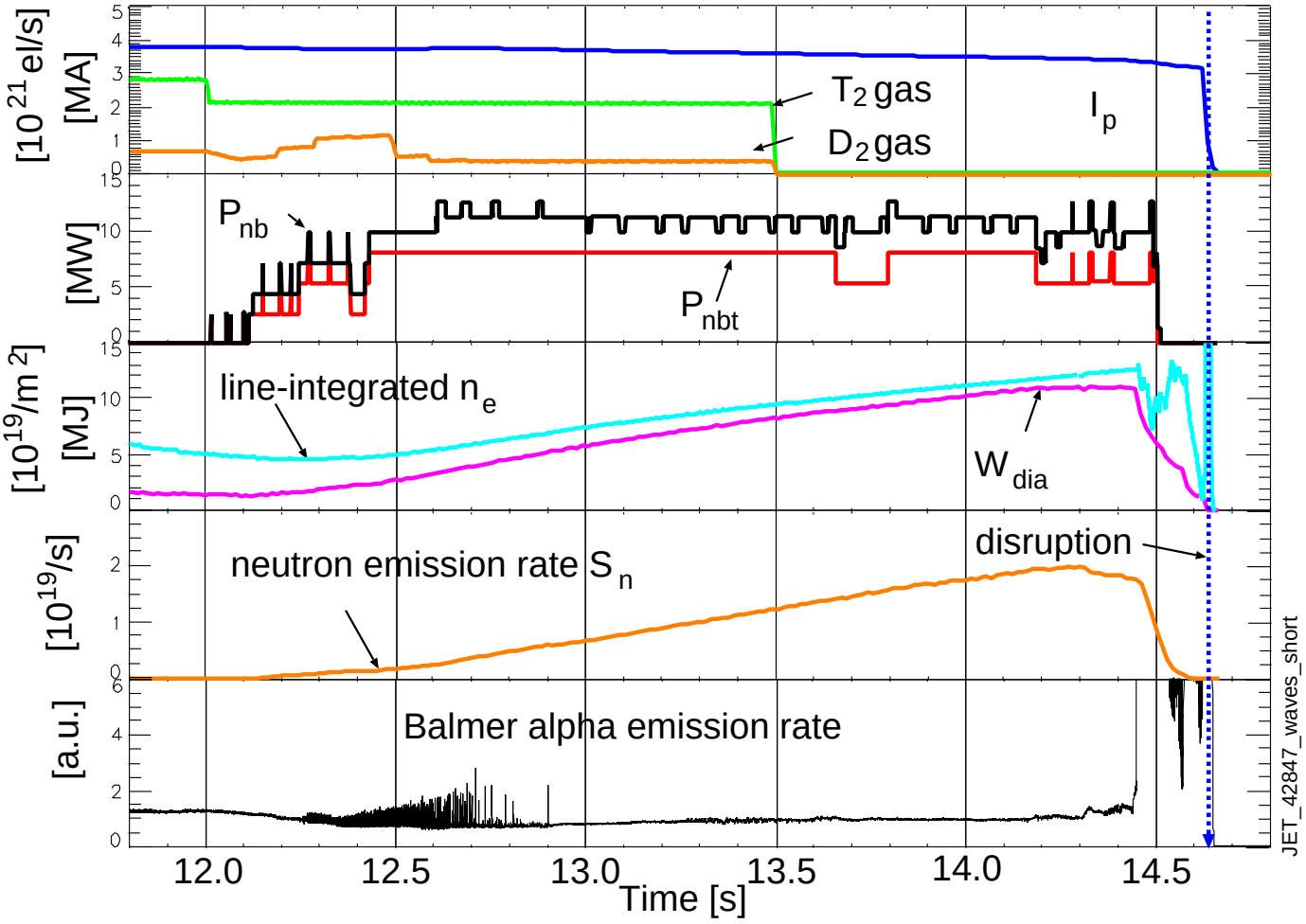

FIG. 7: Waveforms for the JET DT alpha-heating Hot-Ion H-mode discharge 42847 featured in [3, 4] showing the plasma current and gas flow; NBI power and T-NBI power; line-averaged n_e and stored energy; neutron emission rate; and the hydrogenic alpha photon emission. A long duration ELM-free phase is seen between 12.9s and 14.4s. A mode-lock occurred at 14.60 and a disruption at 14.63 s. The P_{nb} waveforms were often choppy. Waveforms for another DT discharge (42856) from the scan are featured in [5].

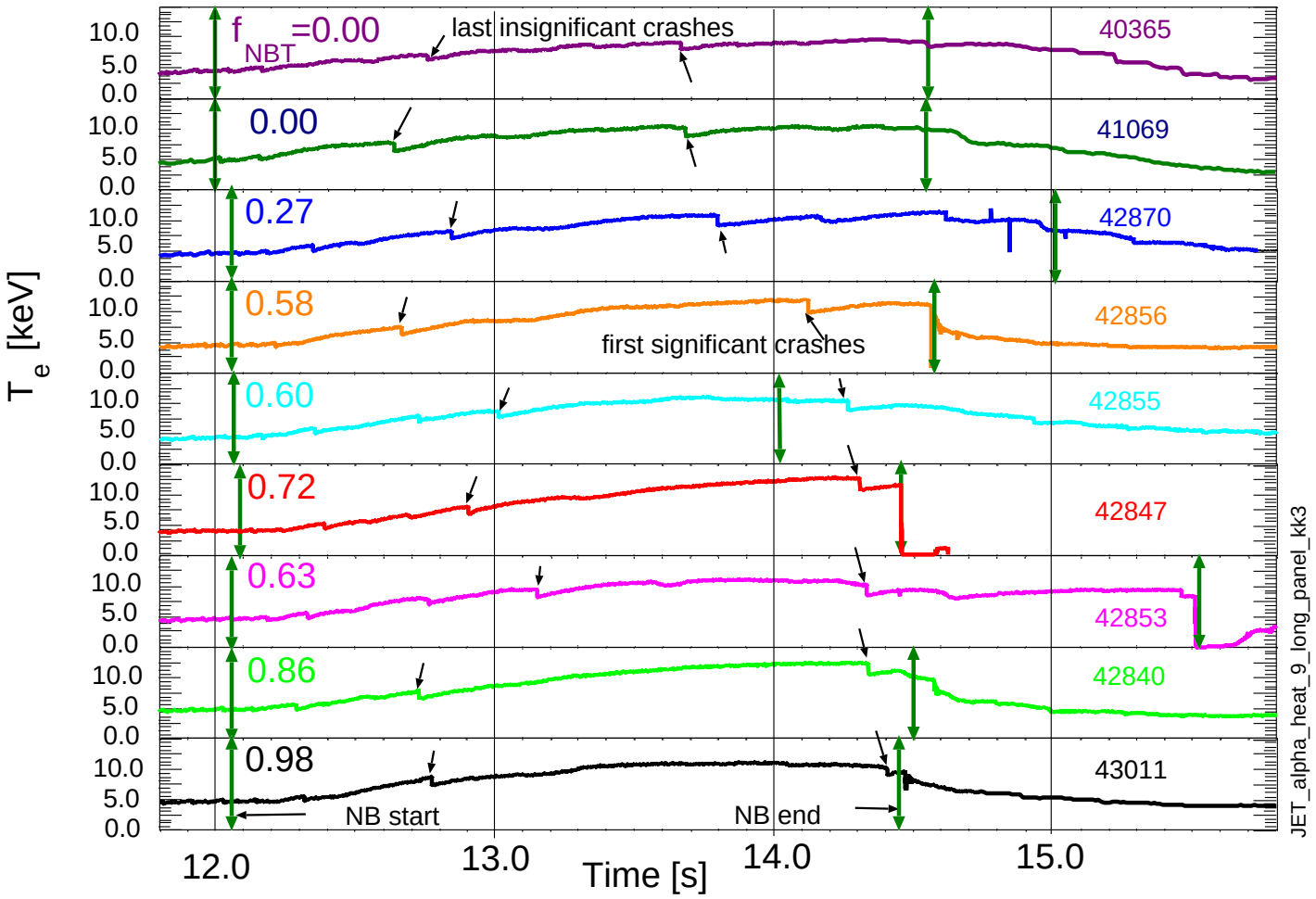

FIG. 8: Waveforms from electron cyclotron emission ECE near the core region showing sawtooth crashes for the JET alpha heating scan. Parameters are given in table 1. Insignificant sawtooth crashes ware seen during the first second or so of NBI which started around 12.0s. The NBI phases are between the vertical double-headed arrows. The discharges are ordered with increasing times of significant sawtooth crashes. The times t_c of the first significant sawtooth crashes increased approximately with increasing $f_{\rm NBT}$ and central $< A >_{\rm hyd}$. Eight of these discharges were shown in figure 3 of [5]. The ELM-free phase ended after the first significant sawtooth for all the discharges.

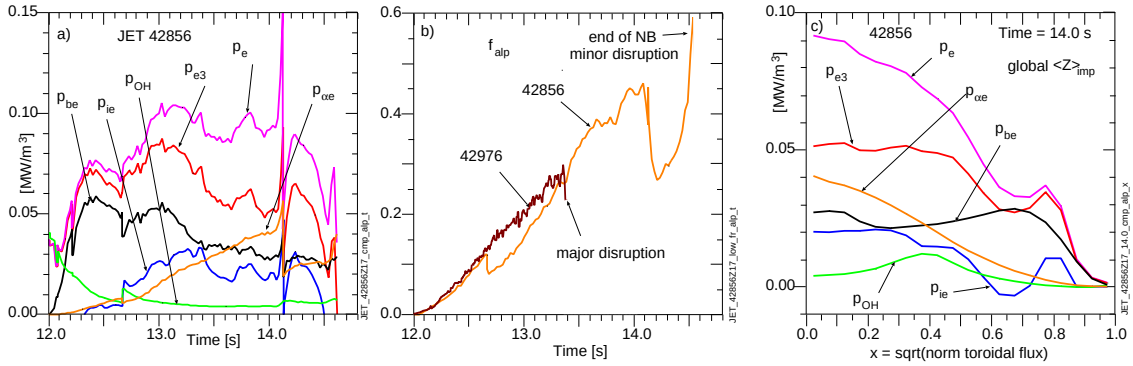

FIG. 9: Electron heating rates: a) time-evolution of the core rates for the JET alpha heating discharge 42856. The spike occurring at a sawtooth crash at 14.12s may be an artifact of the modeling; b) ratio $f_{\rm alp}$ of central $p_{\alpha e}$ and the central total electron heating rates for the alpha heating discharge and for the record $Q_{\rm DT}$ discharge, terminated by a "giant ELM' occurring after 13.4s. The central $p_{\alpha e}$ and $f_{\rm alp}$ in the alpha heating discharge drop at the sawtooth crash 16.14.2s, then start to recover to end of the NB phase, when their values become relatively uncertain; c) profiles of the rates in the flattop phase. The heating rates are less than the TFTR values in figure 2-b) but the ratio $f_{\rm alp}$ is larger.

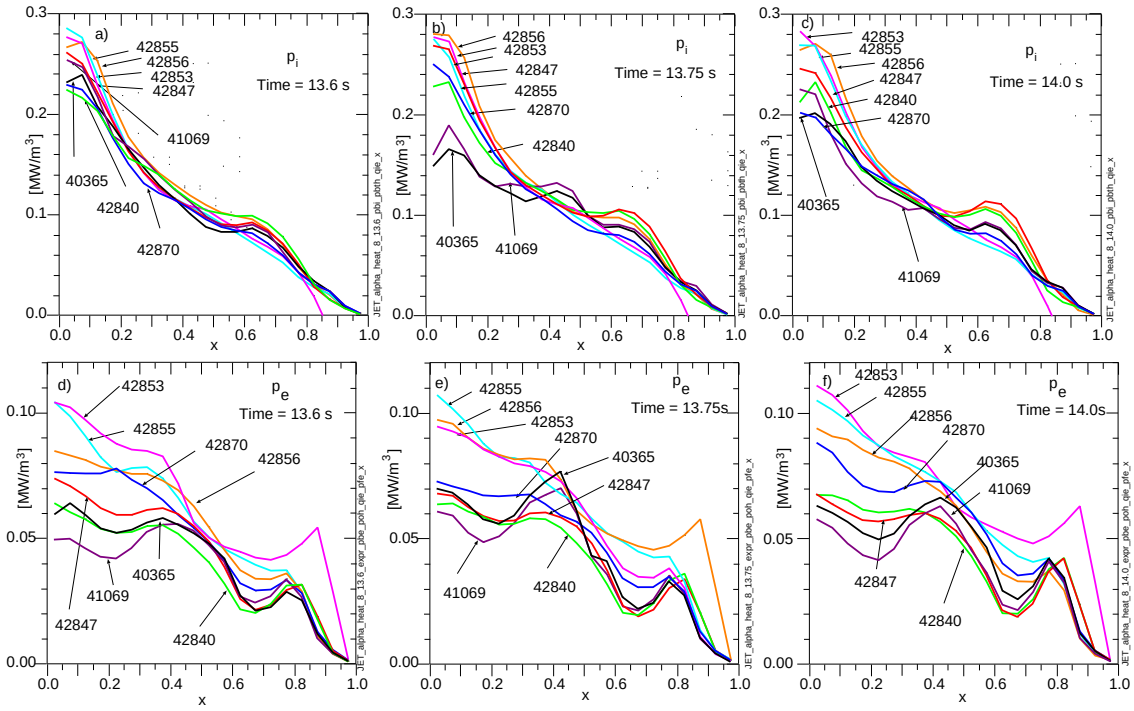

FIG. 10: Profiles of the effective thermal ion total heating rate $p_{\rm i}$ for the JET alpha heating scan at: a) 13.6s; b) 13.75s; and c) 14.0s and of the effective electron heating rate $p_{\rm e}$ at d) 13.6s; e) 13.75s; and f) 14.0s. Values of $p_{\rm bi}$ are much smaller than the TFTR results shown in figure 4. Discharges with higher T fraction $f_{\rm NBT}$ and $< A >_{\rm hyd}$ had higher $p_{\rm i}$ and $p_{\rm e}$. Profiles of $p_{\rm be}$ show a similar hierarchy but are lower than $p_{\rm bi}$ by a factor of five.

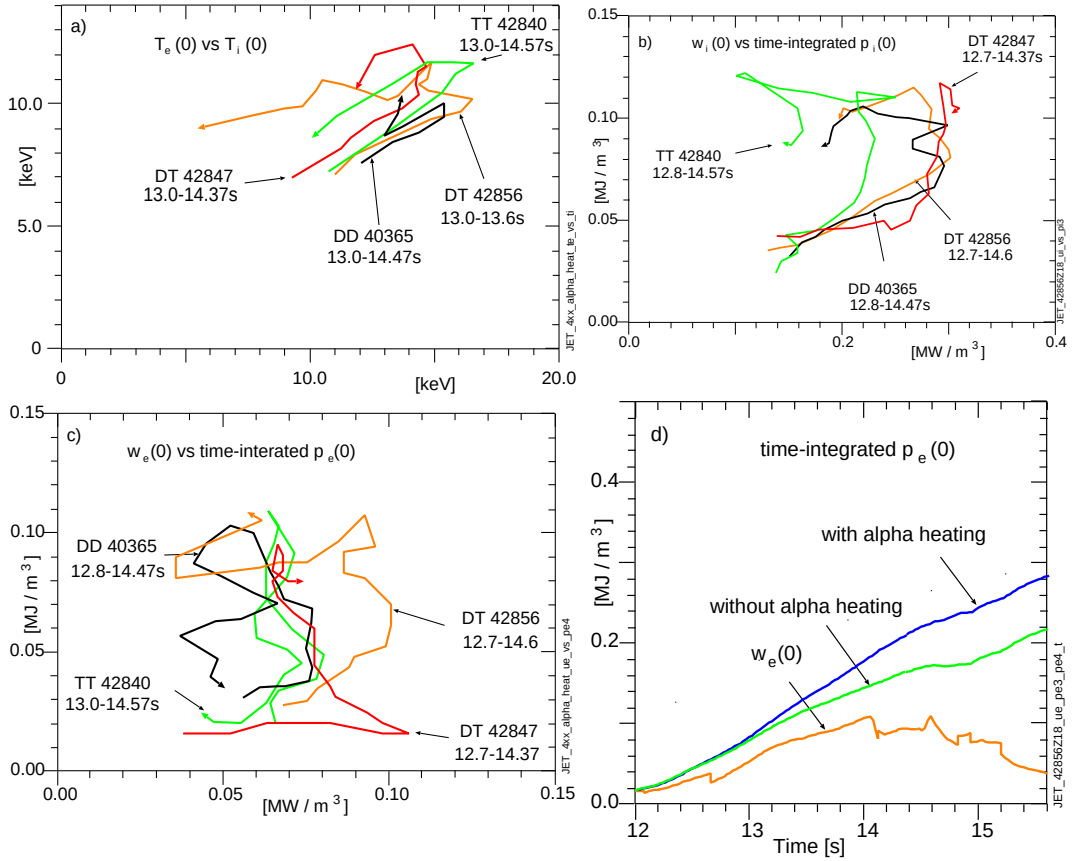

FIG. 11: Trajectories of four of the JET alpha heating discharges: a) central T_e versus T_i; The DD, DT, and TT discharges have similar rates of increase up to maximum T_i as in figure 3. b) central $w_{\rm i}$ vs the time-integrated $p_{\rm i}$. These are more noisy than those in TFTR figure 4-e), but show qualitatively similar isotopic mass effects; c) central $w_{\rm e}$ verses the time-integrated $p_{\rm e}$; and d) comparison of the central $w_{\rm e}$ with the time-integrated $p_{\rm e}$ with and without alpha heating.

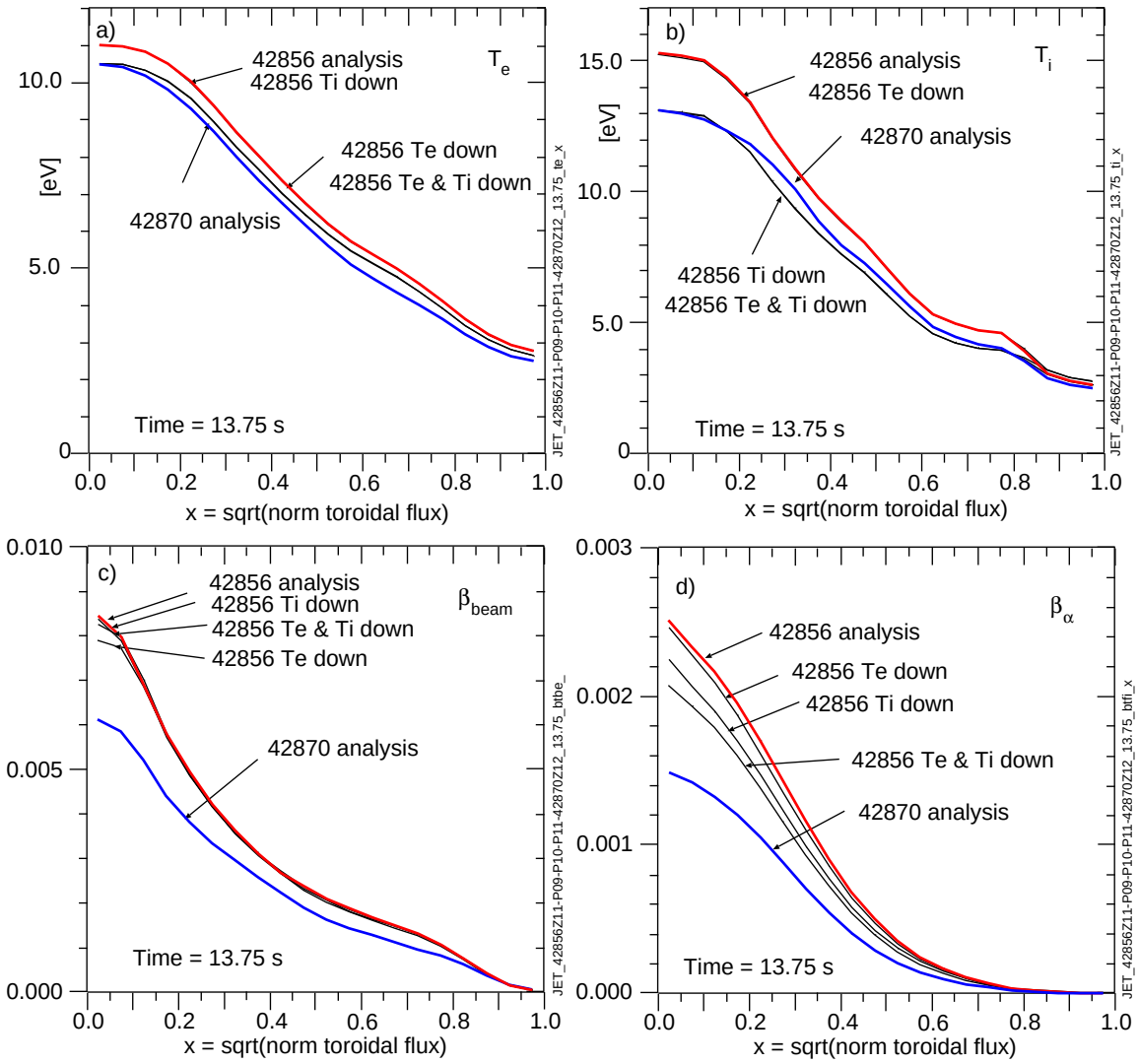

FIG. 12: TRANSP simulations of the JET 42856 with T_e and T_i scaled down to 42870; a) T_e; b) T_i; c) beta toroidal of beam ions; and d) beta toroidal of alpha ions.

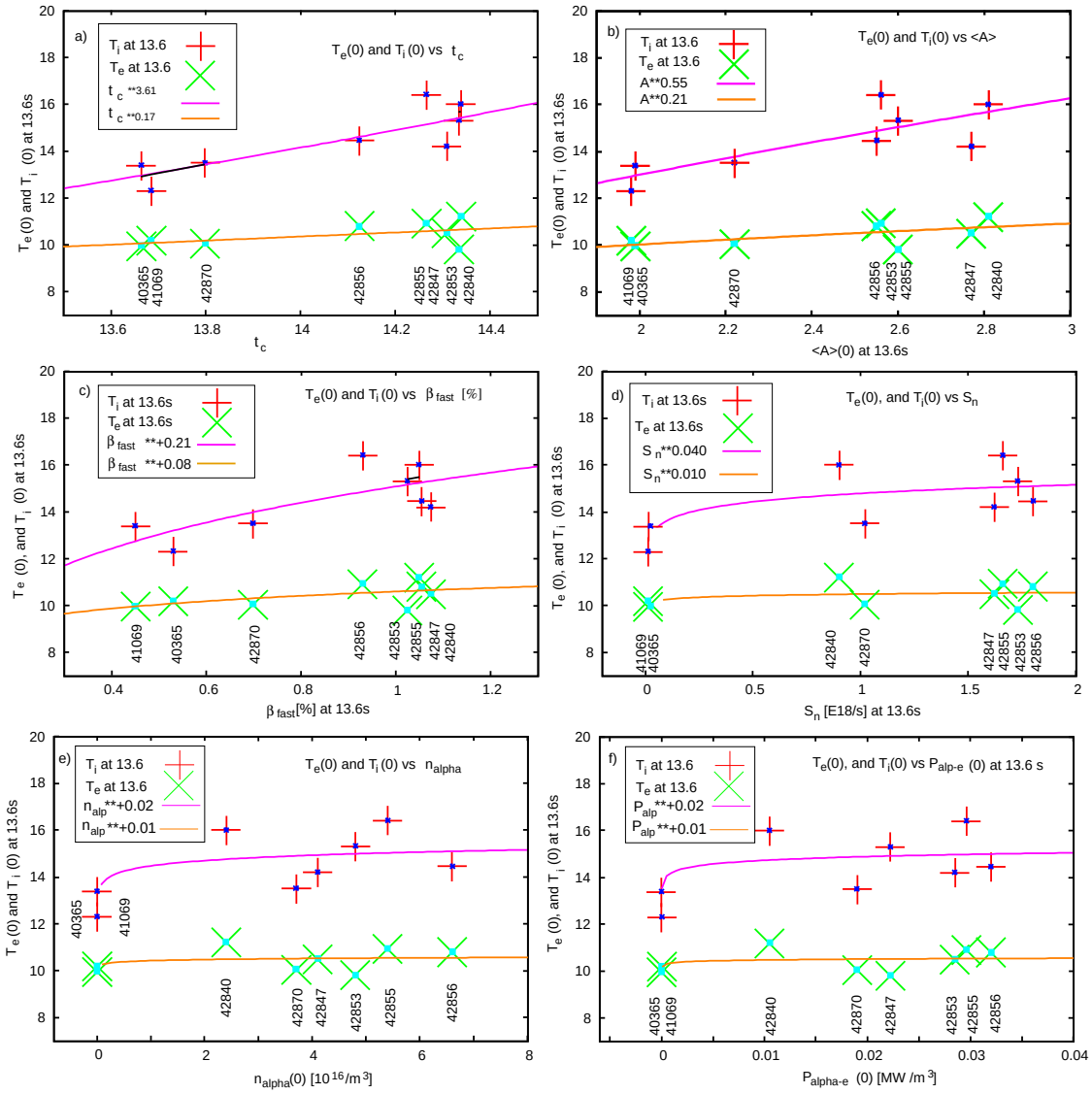

FIG. 13: Central temperatures from the JET alpha heating scan at 13.6s (before the first significant sawtooth crash t_c) vs a) time of the first significant sawtooth crash t_c (at 13.66s); b) central isotopic mass; c) central toroidal beta of the fast beam and alpha ions $\beta_{\rm fast}$; d) neutron emission global rate $S_{\rm n}$; e) central alpha density; and f) central alpha-electron heating rate $p_{\alpha e}$. The scalings in a) are similar to those seen in the delay time δ_t between the last insignificant and the first significant sawtooth crash. The parameters t_c and $S_{\rm n}$ are measured. The others are taken from TRANSP analysis. Power-law fits are shown.

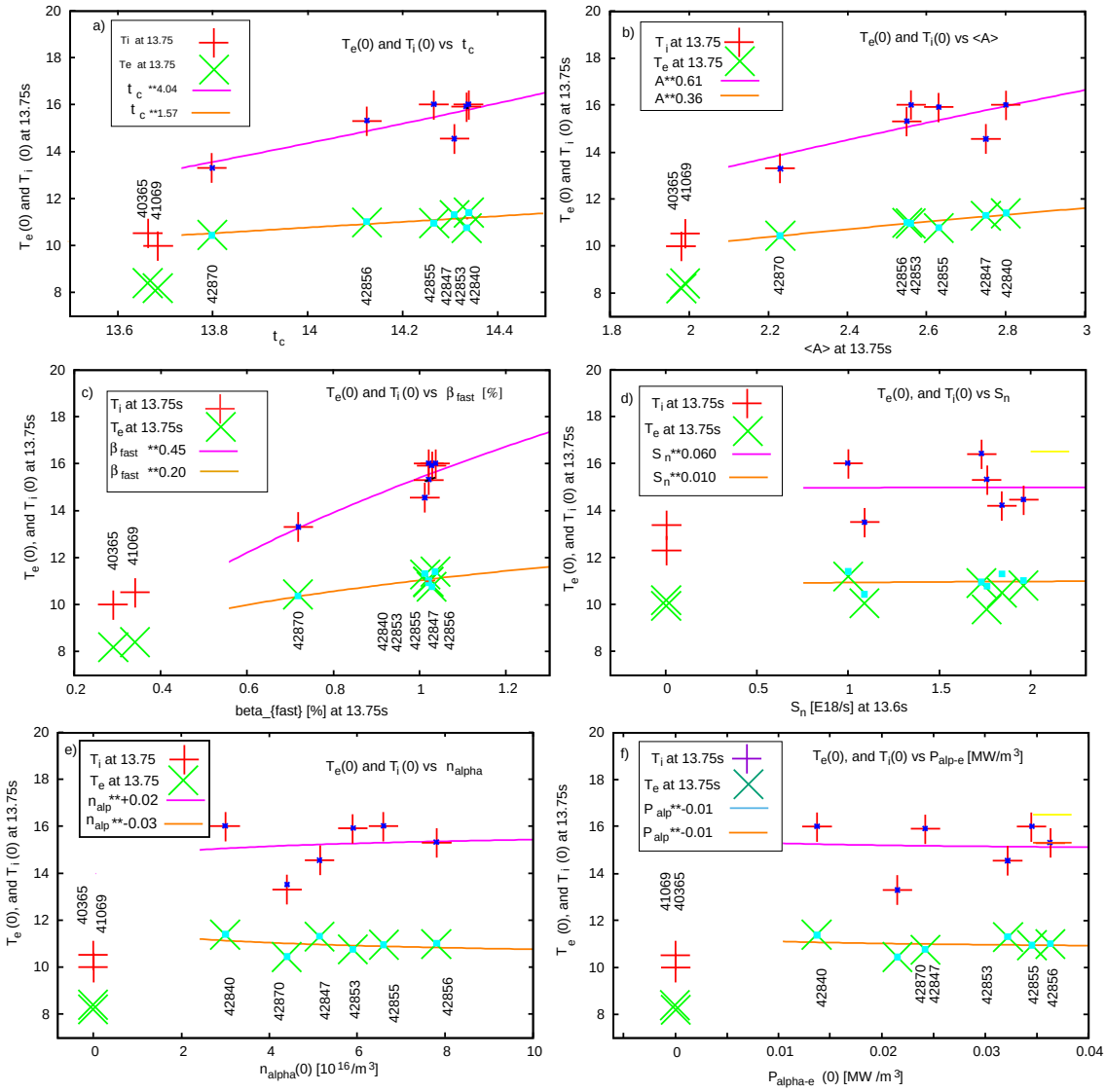

FIG. 14: Central temperatures from the JET alpha heating scan at 13.75s (after both DD discharges experienced significant sawtooth crashes) vs the variables used in figure 13: a) t_c; b) central $< A >_{\rm hyd}$; c) central $\beta_{\rm fast}$; d) $S_{\rm n}$; and f) central alpha density; and central $p_{\alpha e}$. The scalings in c) are comparable to the scalings in figure11a) of [5] normalized to values for discharge 42870 (with $f_{\rm NBT}$=0.27). The scalings in b) are comparable to the scalings in figure11-c) and d) of [5]. The discharge 42856 has MHD which occurred after 13.6s, shown in figure2 of [5].

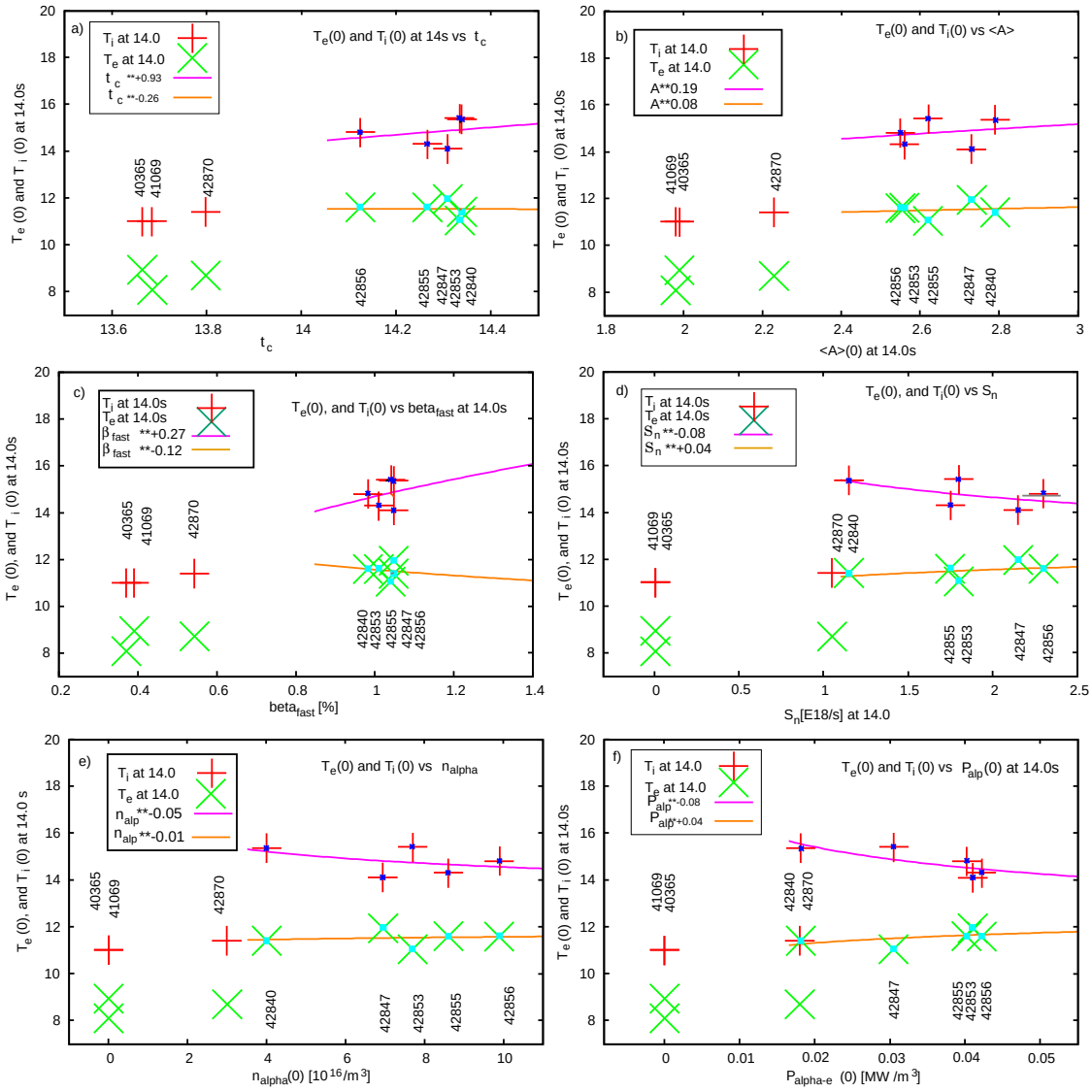

FIG. 15: Central temperatures from the JET alpha heating scan at 14.0s (after three of the discharges experienced their first significant sawtooth crashes) vs the variables used in figure 13 and figure 14: a) t_c; b) central $< A >_{\rm hyd}$; c) neutron emission rate $S_{\rm n}$; e) central alpha density; and e) central alpha-electron heating rate $p_{\alpha e}$.

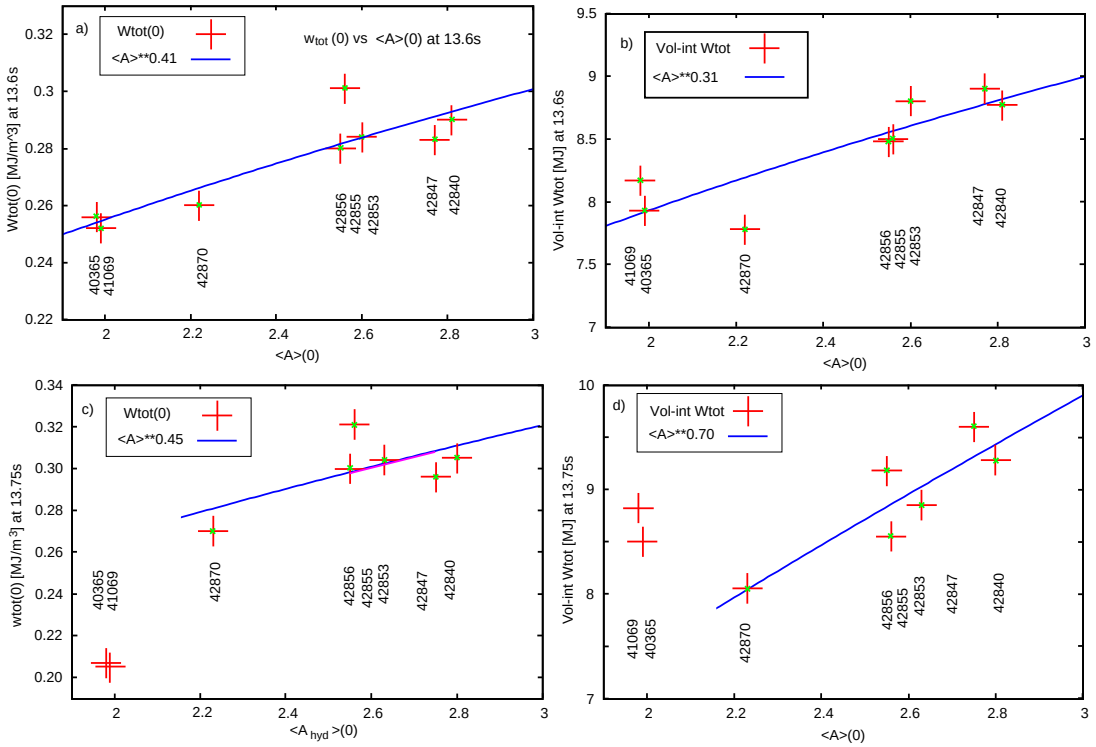

FIG. 16: Scaling with $< A >_{\rm hyd}$ of a) core and b) volume-integrated $w_{\rm tot}$ at 13.6 s; c) core and d) volume-integrated $w_{\rm tot}$ at 13.75s.

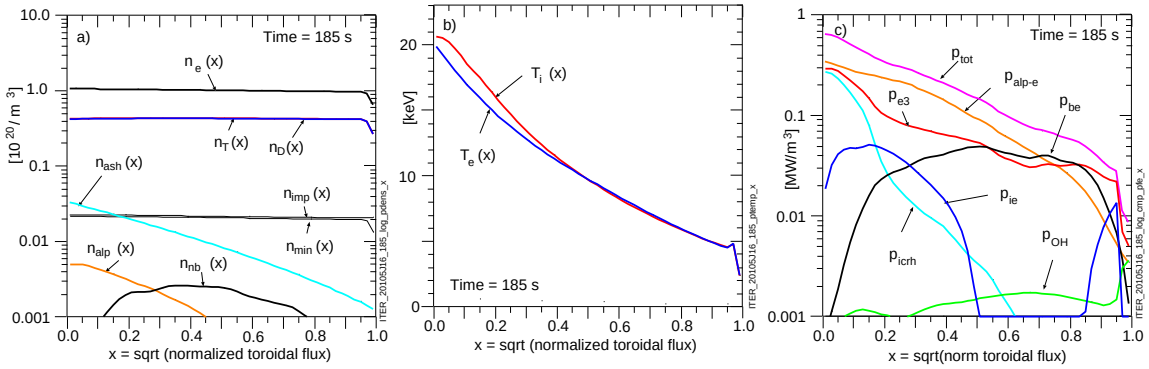

FIG. 17: Predictions for profiles in an ITER ELMy H-mode plasma: a) densities; b) T_e and T_i; and c) electron heating rates.

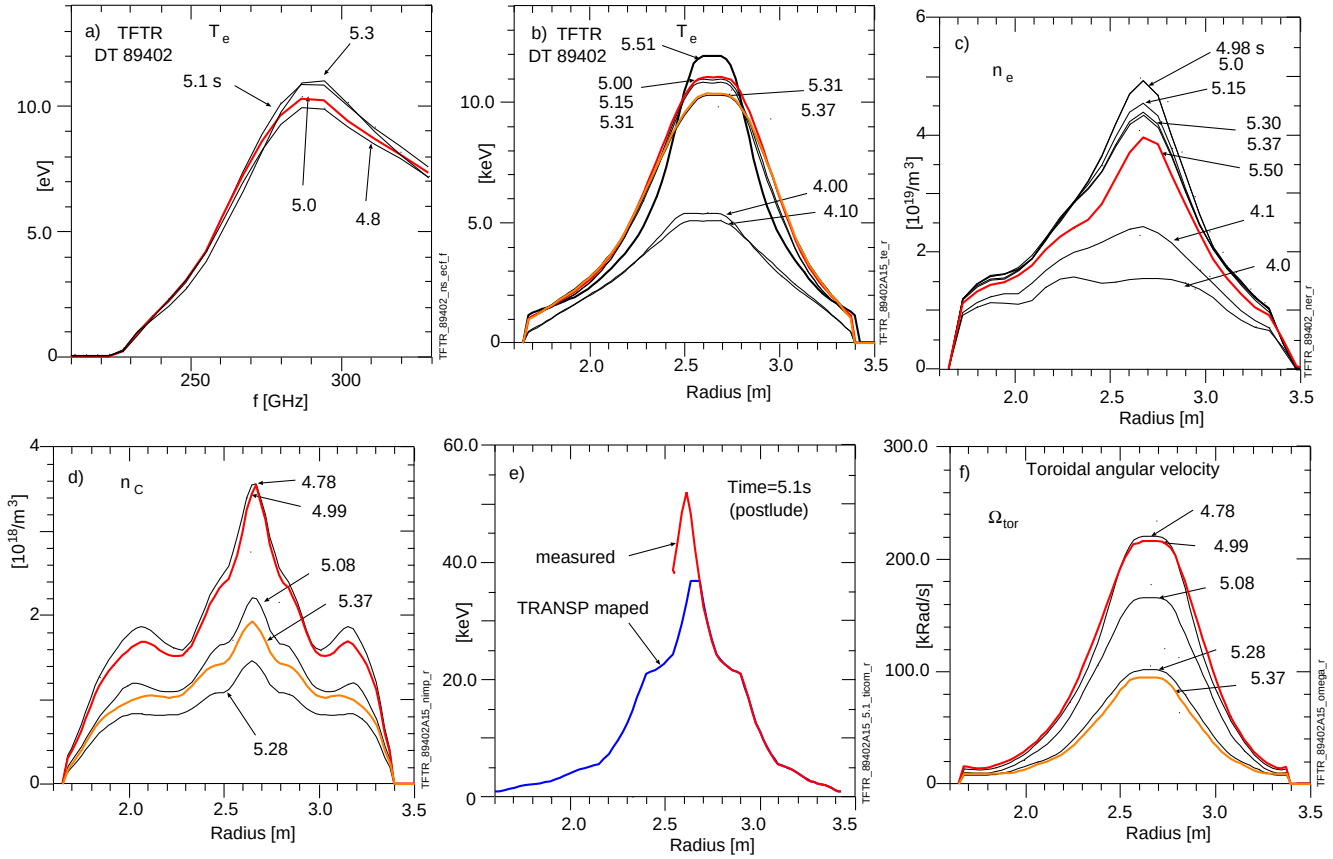

FIG. 18: Input profiles used in the TRANSP analysis of the TFTR DT supershot with a NB postlude phase: a) input electron cyclotron emission ece; to 2.64 m by 5.5 s when the current ramp-down started. b) T_e profiles computed be TRANSP from the ece input; c) n_e profiles from interferometry. Supershots rested on a large toroidally-symmetric inner limiter which caused the n_e profiles were lopsided due to the proximity to the dominant source of wall recycling. The magnetic axis is computed by TRANSP to expand to 2.66 m by 5.0 s, then to shrink The axis is close to that of peaks of T_e and n_e. b) input carbon ion temperature mapped by TRANSP. The CX measurements extended slightly inboard of the magnetic axis. TRANSP used the data only from the axis outward. A mismatch of the TRANSP and CX magnetic axis caused TRANSP to underestimate the peak T_i; d) carbon density n_c from charge-exchange (CX) measurements of carbon; normalized by TRANSP to a well-calibrated visible bremsstrahlung measurement; e) T_i calculated from the input T_c from CX data; and f) comparison of the ion and electron temperatures mapped by TRANSP to its native radial grid of equally spaced square root of normalized toroidal flux, which is approximately the minor radius normalized to the last-closed-flux surface value. T_c is the mapped input carbon temperature and T_i is calculated from T_c assuming local ion-electron energy equilibration [13]. Note the relatively peaked n_e, T_i, and n_c and the broader T_e profiles suggesting a transport barrier in the ion channels and a clamped T_e gradient scale length.

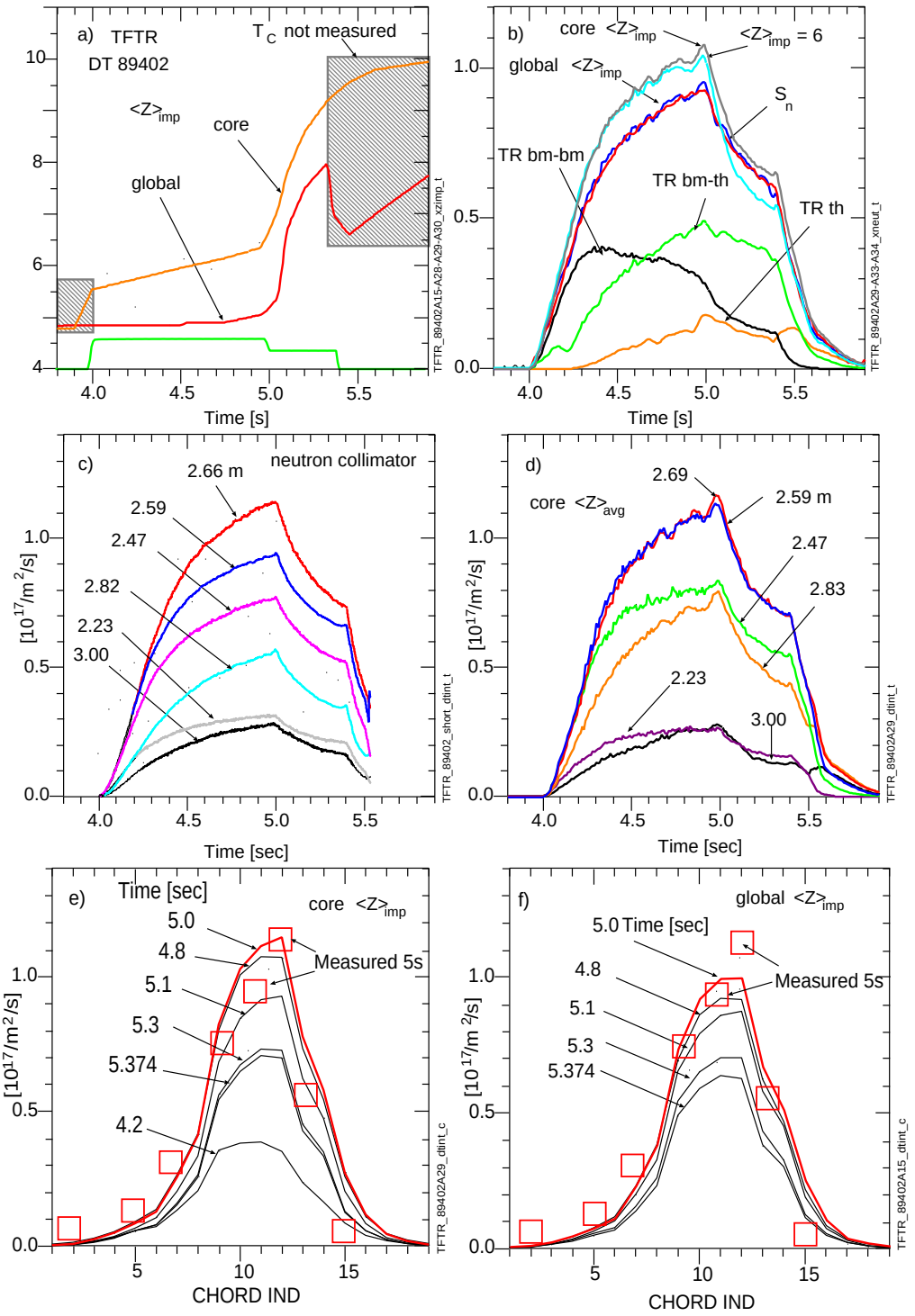

FIG. 19: Comparisons with measurements of TRANSP runs of the TFTR DT 89402 using three values for the charge $< Z >_{\rm imp}$ of an effective one-species impurity ion: a) "core' and "global' $< Z >_{\rm imp}$ fits. Uncertainties in T_i at times without CX measurements have large effects in the fits to the core $Z_{\rm eff}$; b) simulation of the neutron emission rates computed by TRANSP from beam-target, beam-beam, thermonuclear thermal, and their total using the global $< Z >_{\rm imp}$, compared with the measured the measured total $S_{\rm n}$. The totals assuming the core $< Z >_{\rm imp}$ and $< Z >_{\rm imp}$=6.0 are also shown; The core $< Z >_{\rm imp}$ simulation of $S_{\rm n}$ is 10% higher; c) chordal neutron emission rate measured by the neutron collimator diagnostic; d) and e) TRANSP core $< Z >_{\rm imp}$ simulations of the chordal neutron emission; and f) global $< Z >_{\rm imp}$ simulations are lower in the core. Both simulations of the profiles are narrower than measured. Fast ion anomalous diffusion (not assumed here) could spread the beam ions and thus the neutron emission rate profiles spatially.

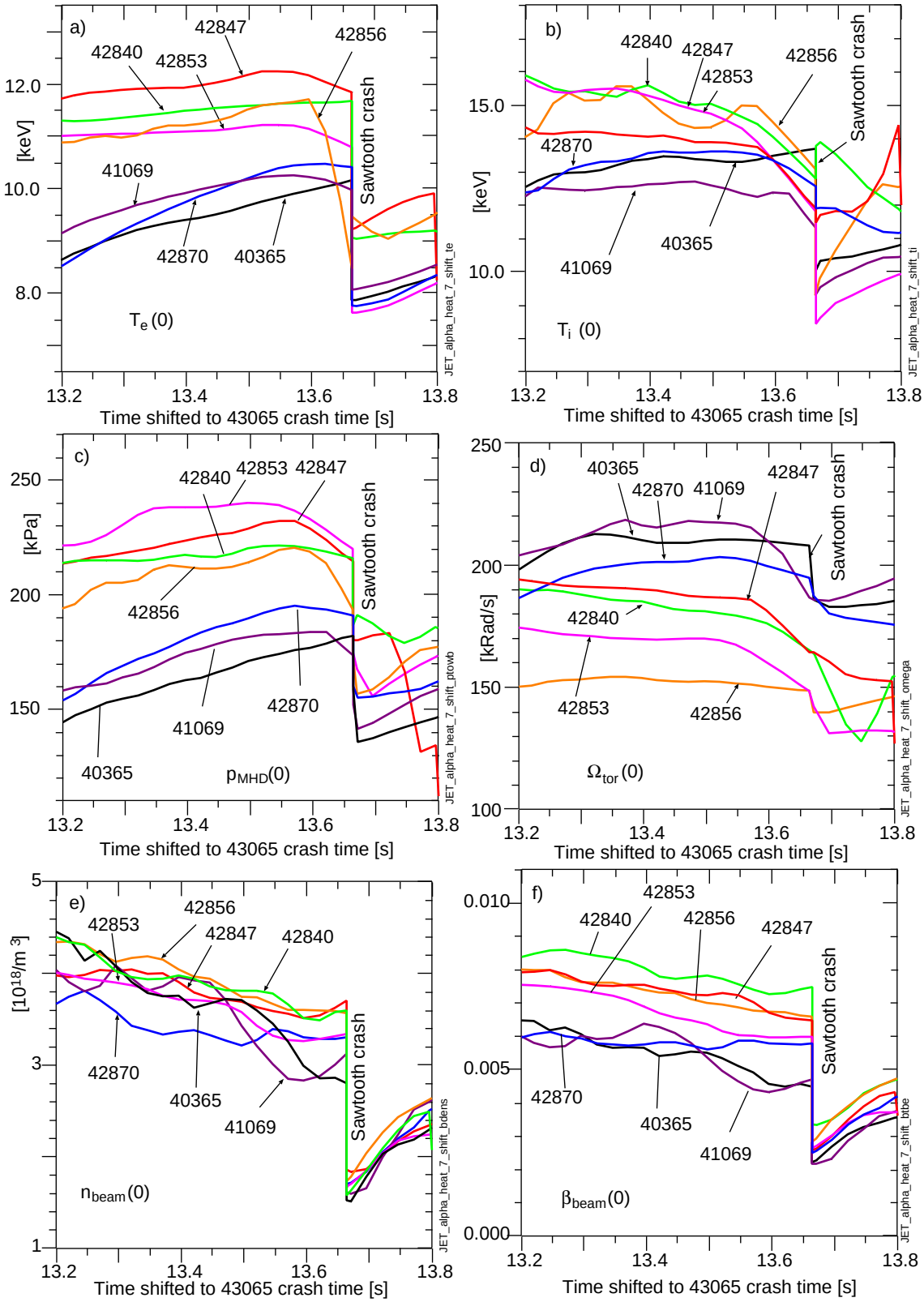

FIG. 20: Central plasma parameters from he JET alpha heating scan time-shifted to the time of the first significant sawtooth crash (in discharge 40365): a) MHD pressure (thermal plus fast particle plus rotation energy densities); b) electron temperature; c) hydrogenic ion temperature; d) toroidal rotation of carbon impurity ions; e) fast beam ion density; and f) beam ion toroidal pressure.